mTORC1 signaling in antigen-presenting cells of the skin restrains CD8(+) T cell priming

Pelgrom, L.R.; Patente, T.A.; Otto, F.; Nouwen, L.V.; Ozir-Fazalalikhan, A.; Ham, A.J. van der; ... ; Everts, B.

Cell Reports

Article

mTORC1 signaling in antigen-presenting cells of the skin restrains CD8$^+$ T cell priming

Graphical abstract

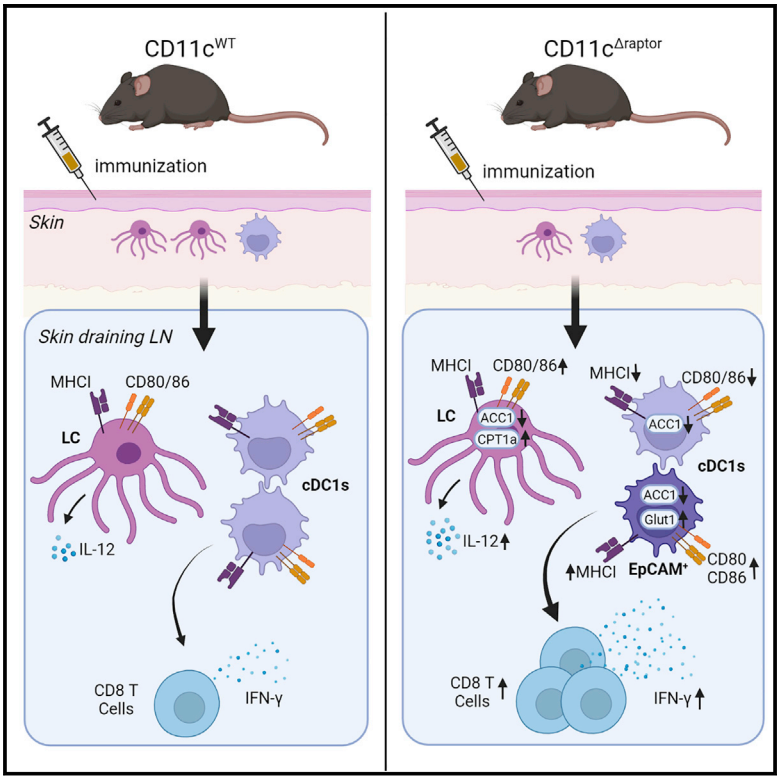

Highlights

- mTORC1 regulates DC metabolism and activation in a DC subset-specific manner
- Cross-presentation by cDC1s is supported by mTORC1 signaling
- CD8$^+$ T cell priming following immunization is enhanced in CD11c$^{\Delta raptor}$ mice
- This is associated with accumulation of an immunogenic EpCAM$^+$ cDC1 subpopulation

Authors

Leonard R. Pelgrom, Thiago A. Patente, Frank Otto, ..., Graham A. Heieis, Ramon Arens, Bart Everts

Correspondence

b.everts@lumc.nl

In brief

How mTORC1 regulates dendritic cell (DC) biology *in vivo* is unclear. Pelgrom et al. demonstrate that DC-specific mTORC1 deficiency potentiates immunization-induced CD8$^+$ T cell responses. This is linked to alterations in DC metabolism and increased immunogenicity of an EpCAM$^+$ cDC1 subpopulation. Thus, targeting mTORC1 may help to boost vaccination responses.

Pelgrom et al., 2022, Cell Reports *40*, 111032
July 5, 2022
https://doi.org/10.1016/j.celrep.2022.111032

Cell Reports

CellPress
OPEN ACCESS

Article

mTORC1 signaling in antigen-presenting cells of the skin restrains CD8$^+$ T cell priming

Leonard R. Pelgrom,[1,3] Thiago A. Patente,[1,3] Frank Otto,[1] Lonneke V. Nouwen,[1] Arifa Ozir-Fazalalikhan,[1] Alwin J. van der Ham,[1] Hendrik J.P. van der Zande,[1] Graham A. Heieis,[1] Ramon Arens,[2] and Bart Everts[1,4,*]

[1]Department of Parasitology, Leiden University Medical Center, Leiden, the Netherlands
[2]Department of Immunology, Leiden University Medical Center, Leiden, the Netherlands
[3]These authors contributed equally
[4]Lead contact
*Correspondence: b.everts@lumc.nl
https://doi.org/10.1016/j.celrep.2022.111032

SUMMARY

How mechanistic target of rapamycin complex 1 (mTORC1), a key regulator of cellular metabolism, affects dendritic cell (DC) metabolism and T cell-priming capacity has primarily been investigated *in vitro*, but how mTORC1 regulates this *in vivo* remains poorly defined. Here, using mice deficient for mTORC1 component raptor in DCs, we find that loss of mTORC1 negatively affects glycolytic and fatty acid metabolism and maturation of conventional DCs, particularly cDC1s. Nonetheless, antigen-specific CD8$^+$ T cell responses to infection are not compromised and are even enhanced following skin immunization. This is associated with increased activation of Langerhans cells and a subpopulation of EpCAM-expressing cDC1s, of which the latter show an increased physical interaction with CD8$^+$ T cells *in situ*. Together, this work reveals that mTORC1 limits CD8$^+$ T cell priming *in vivo* by differentially orchestrating the metabolism and immunogenicity of distinct antigen-presenting cell subsets, which may have implications for clinical use of mTOR inhibitors.

INTRODUCTION

Dendritic cells (DCs) of the innate immune system are uniquely equipped to present antigens, costimulatory molecules, and polarizing cytokines to T cells. This gives DCs a central role in the establishment of both protective adaptive immunity following infections and vaccination and tolerance through induction of anergy to host self-antigens and regulatory T cells (Kapsenberg, 2003). DCs patrol tissues until they encounter danger signals, which is followed by rapid changes in their biology that enable them to efficiently migrate to lymphoid tissues and appropriately instruct the T cells there (Eisenbarth, 2019). As these changes require concomitant changes in cellular metabolism (Patente et al., 2019), manipulation of DC metabolism may become an attractive therapeutic strategy for controlling the outcome of immune responses.

Mechanistic target of rapamycin (mTOR) coordinates intracellular metabolism with environmental inputs that include nutrients, growth factors, and immunological cues such as cytokines. It is a protein complex that exists in two distinct forms with either raptor (mTOR complex 1 [mTORC1]) or rictor (mTORC2) as one if its core components. While mTORC2 signaling governs proliferation, survival, and cytoskeletal remodeling, mTORC1 activity promotes increased protein synthesis and anabolic metabolism of lipids, nucleotides, and glucose and reduces autophagy (Saxton and Sabatini, 2017). mTORC1 signaling has been shown to be vital for the metabolic reprogramming of various immune cells (Jones and Pearce, 2017; Weichhart et al., 2015). The role of mTORC1 in DC biology has been extensively studied *in vitro* and seems to be context- and species-dependent (Snyder and Amiel, 2018; Weichhart et al., 2015). *In vivo*-transferred murine bone-marrow-derived DCs (BMDCs) were shown to prime stronger CD8$^+$ T cell responses after toll-like receptor (TLR) triggering in the presence of rapamycin (Amiel et al., 2012; Jagannath and Bakhru, 2012; Jagannath et al., 2009). This was associated with increased autophagy (Jagannath et al., 2009), a switch from anaerobic glycolysis to oxidative phosphorylation (Amiel et al., 2014), increased longevity, and maintenance of high costimulatory molecule expression (Amiel et al., 2012). These middle two are likely secondary to autocrine effects of mTOR-controlled TLR-induced nitric oxide (NO) production (Everts et al., 2012; Lawless et al., 2017), so whether these findings translate to conventional DCs (cDCs) that express little NO *in vivo* (Thwe and Amiel, 2018) is currently unclear.

Thus far, *in vivo* studies using CD11c-cre raptor$^{fl/fl}$ (CD11c$^{\Delta raptor}$) mice that display a selective loss of mTORC1 signaling in CD11c-expressing cells, which is largely restricted to DCs, revealed that homeostasis of CD103$^+$ type 1 conventional DCs (cDC1s) in the lungs (Sinclair et al., 2017) and Langerhans cells (LCs) in the skin was critically dependent on mTORC1 signaling. Maintenance of LCs in draining lymph nodes (Kellersch and Brocker, 2013), CD8$^+$ cDC1s in the spleen, and CD11b$^+$ cDC2s in the lamina propria (Ohtani et al., 2012) are also affected but to a lesser degree. Functionally, mice with a CD11c-specific mTOR deletion, in which both mTORC1 and mTORC2 signaling is compromised, have an antigen-presenting cell (APC)

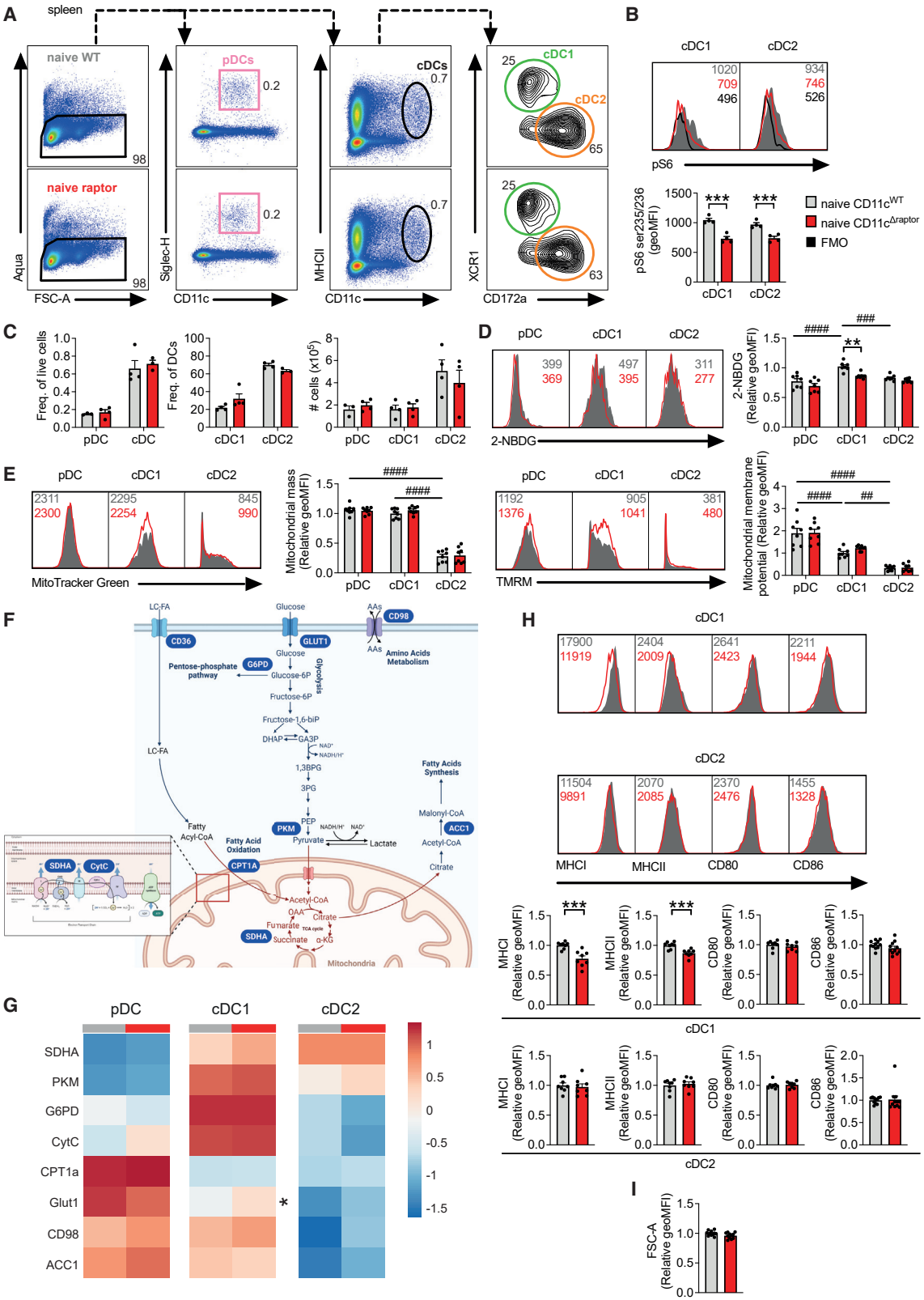

(legend on next page)

compartment in the lung with altered cellular metabolism. This was associated with a reduced capacity to mount a $CD8^+$ T cell response upon viral infection and was directly responsible for a shift from mounting a type 2 to a type 17 immune response following allergen challenge (Sinclair et al., 2017). However, whether these effects are a consequence of a defect in mTORC1 signaling, mTORC2, or both, remains unclear. Hence, while the role of mTORC1 signaling in DCs in regulating their metabolic and T cell-priming capacity has been extensively studied *in vitro*, the role of specifically mTORC1 signaling in regulating DC metabolism and T cell-priming function *in vivo* remains to be addressed.

In the current study, we found that the loss of raptor in DCs alters metabolic properties and compromises the maturation of different DC subsets in the spleen and skin-draining lymph nodes to various degrees, which was apparent during steady-state conditions, systemic infection, and local immunization. These effects were most pronounced in cDC1s. Nevertheless, the priming of $CD8^+$ T cells was not impaired but rather potentiated following subcutaneous (s.c.) immunization. This latter finding was associated with an enhanced activation phenotype of LCs and a subpopulation of cDC1s expressing EpCAM, of which the latter showed increased physical interactions with $CD8^+$ T cells *in vivo*. Together, these data reveal APC subset-specific effects of loss of mTORC1 signaling and how this controls T cell responses *in vivo*, with a potential role for mTORC1 in restricting cDC1-dependent $CD8^+$ T cell priming.

RESULTS

mTORC1 signaling impacts glucose uptake and major histocompatibility complex (MHC) expression by splenic cDC1s

Mice with a conditional deletion of raptor in CD11c-expressing cells ($CD11c^{\Delta raptor}$) displayed decreased steady-state phosphorylation of ribosomal protein S6, a downstream target of mTORC1, in both splenic cDC1s and cDC2s (Figure 1B). T cells and B cells were not affected (Figure S1A). In contrast to what was previously reported (Ohtani et al., 2012), the frequency and numbers of splenic cDC1s were similar between CD11c-cre-negative ($CD11c^{WT}$) and $CD11c^{\Delta raptor}$ littermates (Figures 1A and 1C). We did, however, observe changes in their metabolism. In keeping with reports that splenic cDC1s are more metabolically active than splenic cDC2s (Du et al., 2018), cDC1s were found to have higher uptake of the fluorescent glucose analog 2-NBDG than other splenic DC subsets under steady-state conditions (Figure 1D). And consistent with a well-described role for mTORC1 signaling in supporting glycolysis (Jones and Pearce, 2017; Saxton and Sabatini, 2017; Snyder and Amiel, 2018; Weichhart et al., 2015), deletion of raptor lowered 2-NBDG uptake in cDC1s but not in cDC2s and plasmacytoid DCs (pDCs) (Figure 1D). Loss of raptor did not affect mitochondrial mass or membrane potential (Figure 1E). To more fully characterize changes in cellular metabolism, we developed an antibody panel for spectral flow cytometry that includes rate-limiting metabolic enzymes in key metabolic pathways (Met-flow, highlighted in blue in Figure 1F) (Ahl et al., 2020; Heieis et al., 2022). In support of higher metabolic activity of cDC1s compared with cDC2s, they displayed overall higher metabolic enzyme expression (Figure 1G). Also, consistent with literature (Wu et al., 2016), pDCs showed highest expression of carnitine palmitoyltransferase 1a (CPT1a), a transporter involved in mitochondrial fatty acid oxidation. Loss of mTORC1 signaling in splenic DCs did not alter the expression of the tested metabolic enzymes, except for glucose transporter 1 (GLUT1) in cDC1s. However, in line with the importance of glycolysis for DC maturation (Everts et al., 2014; Guak et al., 2018; Thwe et al., 2017), reduced 2-NBDG uptake was accompanied by impaired MHC class I and class II surface expression in raptor-deficient cDC1s but not cDC2s (Figure 1H). This was not secondary to a smaller cell size, as forward scatter of cDC1s was not significantly affected by loss of raptor (Figure 1I).

$CD8^+$ T cell priming in response to, and protection against, listeria infection is intact in $CD11c^{\Delta raptor}$ mice

Given the critical role for cDC1s in the priming and maintenance of $CD8^+$ T cells (Hildner et al., 2008), we next assessed whether reduced MHC class I expression by raptor-deficient splenic cDC1s would affect the $CD8^+$ T cell pool of $CD11c^{\Delta raptor}$ mice. Indeed, in naïve $CD11c^{\Delta raptor}$ mice, antigen-experienced effector (EFF; $CD44^+CD62L^-$) $CD8^+$ T cells were reduced in blood, and central memory (CM; $CD44^+CD62L^+$) $CD8^+$ T cells were reduced in spleen, despite normal T cell development in the thymus (Figures 2A, S1B, and S1C). As no significant changes in $CD4^+$ T cell populations were found (Figures 2A, S1B, and S1C), reduced MHC class II expression by raptor-deficient splenic cDC1s seems to have no functional consequence in naïve $CD11c^{\Delta raptor}$ mice.

Next, to determine whether $CD8^+$ T cell responses in $CD11c^{\Delta raptor}$ mice would be compromised in response to infection, mice were challenged with an ovalbumin-expressing live-attenuated strain of *Listeria monocytogenes* (Lm-ΔActA-OVA),

Figure 1. mTORC1 signaling is required for glucose uptake by splenic cDC1s and their MHC expression

(A) Flow gating strategy for splenic DC subsets.

(B) Flow-cytometry-based analysis of S6 phosphorylation on serine 235/236 in splenic cDCs from $CD11c^{WT}$ mice in gray, $CD11c^{\Delta raptor}$ mice in red, and a fluorescence minus one (FMO) control in black.

(C) Frequencies and numbers of splenic DC subsets as gated in (A) are enumerated.

(D) Flow-cytometry-based analysis of uptake of fluorescent glucose analog 2-NBDG by splenic DC subsets.

(E) Flow-cytometry-based analysis of mitochondrial mass and mitochondrial membrane potential in splenic DC subsets using MitoTracker Green and TMRM, respectively.

(F) Schematic of core metabolic pathways in which metabolic proteins, analyzed for their expression by spectral flow cytometry, are indicated in blue.

(G) Heatmap displaying the expression of metabolic targets in splenic DC subsets. Expression levels for each marker are shown relative to all DC subsets.

(H and I) Flow-cytometry-based analysis of MHC class I, MHC class II, CD80, and CD86 surface protein expression (H) or forward scatter (FSC; I) of splenic cDCs. Bars represent mean ± SEM of indicated datapoints from individual mice. Unpaired Student's t test (B, H, and I) and two-Way ANOVA (C–E) were used to assess statistically significant differences. Data are from 1 out of 2 representative experiments (B, C, and G) or normalized geoMFI from a pool of 2 (D and E) or 3 (G–I) independent experiments using 3–4 mice per group.

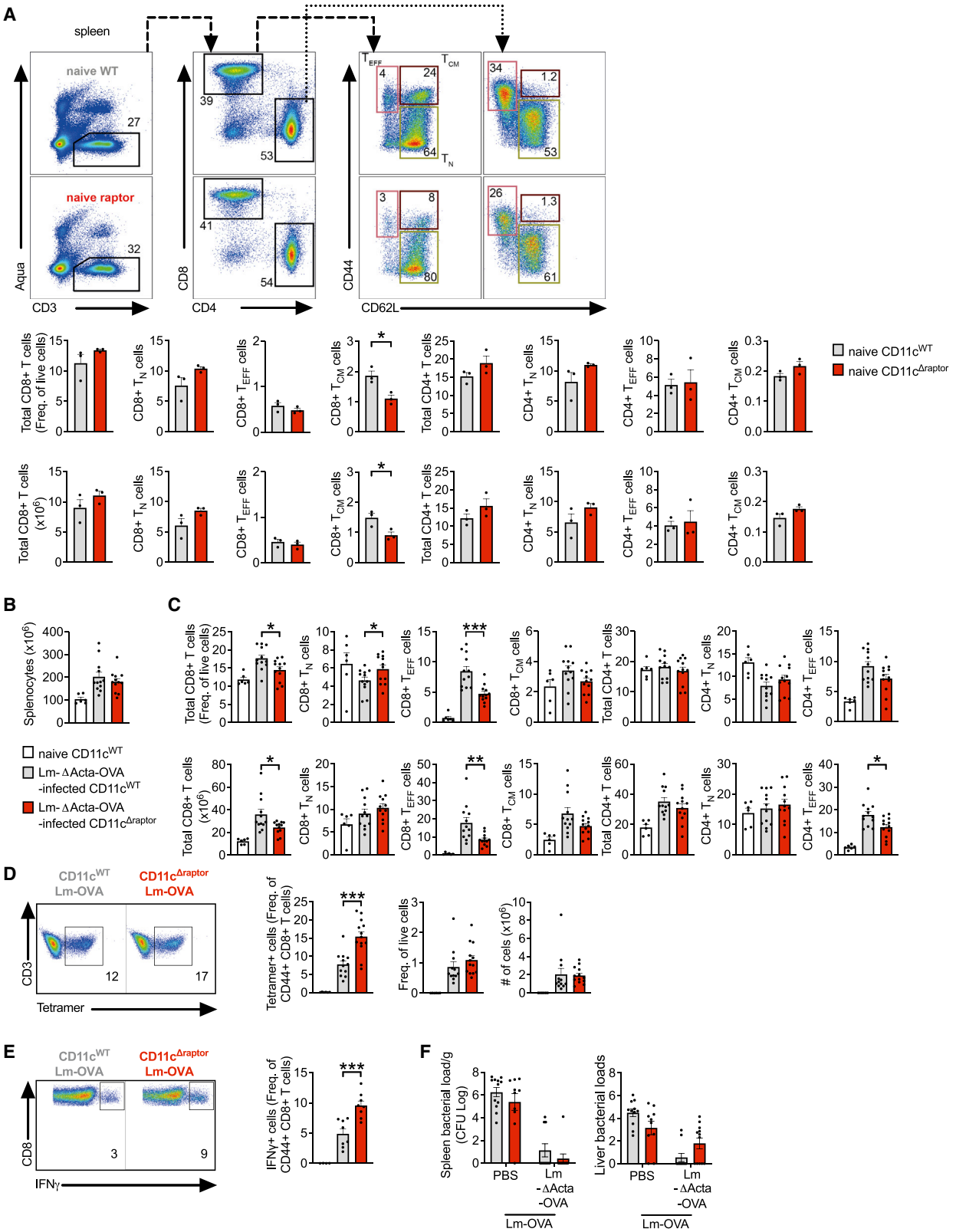

(legend on next page)

a bacterium that primarily infects spleen and liver and depends on splenic cDC1s for $CD8^+$ T cell-mediated clearance (Chávez-Arroyo and Portnoy, 2020). While the overall expansion of effector $CD44^+CD8^+$ T cells in spleens of $CD11c^{\Delta raptor}$ mice was less pronounced (Figures 2B and 2C), the frequency of OVA-specific $CD8^+$ T cells within this effector pool was increased (Figure 2D), resulting in a comparable expansion of OVA-specific $CD8^+$ T cells in $CD11c^{\Delta raptor}$ mice as in $CD11c^{WT}$ mice (Figure 2D). Expansion of effector $CD44^+CD4^+$ T cells was minimally affected (Figure 2C), and their capacity to produce cytokines was unaltered (Figure S1D). In contrast, the production of the prototypical $CD8^+$ cytotoxic T cell (CTL) cytokine interferon-gamma (IFN-γ) by $CD44^+CD8^+$ T cells in spleens from $CD11c^{\Delta raptor}$ mice was higher after *ex vivo* restimulation with OVA (Figure 2E). Together, this suggests that the ability of $CD11c^{\Delta raptor}$ mice to mount antigen-specific $CD8^+$ T cell responses to Lm-ΔActA-OVA infection was not compromised.

To assess whether these changes in the $CD8^+$ T cell compartment would affect protection against a secondary infection, Lm-ΔActA-OVA-infected mice were challenged with replication-competent Lm-OVA 3 weeks later. Frequencies of OVA-specific CM $CD8^+$ T cells 1 day before challenge (d20) and effector $CD8^+$ T cells 3 days after challenge were not affected by loss of raptor (Figure S1E). In line with these results, bacterial loads in spleen and liver did not significantly differ between the two groups (Figure 2F), suggesting that $CD8^+$ T cell memory formation and protective immunity to Lm are not affected by the loss of raptor in $CD11c^+$ cells.

mTORC1 signaling is required for cross-presentation but is dispensable for longevity, maturation duration, and cytokine production by splenic cDCs

To understand how $CD11c^{\Delta raptor}$ mice displayed an intact antigen-specific $CD8^+$ T cell response to Lm infection, despite having cDC1s with decreased surface expression of MHC class I, we assessed how infection affected the metabolism, maturation, and cross-priming function of splenic DCs. Raptor-deficient splenic cDC1s maintained a decreased surface expression of MHC class I following infection with Lm-ΔActA-OVA (Figure 3A). This occurred despite restoration of their ability to take up 2-NBDG (Figure S2A), making glucose uptake, mitochondrial membrane potential, and mitochondrial mass comparable between raptor-deficient and -competent splenic cDC1s during Lm infection (Figure S2A). Additionally, we performed dimensional reduction and unsupervised clustering on data generated from our Met-flow panel for a more detailed metabolic characterization of splenic DCs of 24 h-infected mice. Within cDC1 and cDC2 populations (Figure 3B), we could identify several phenotypically distinct clusters (Figures 3C and 3D), of which the frequency of cDC1 cluster PG-06 was increased and cDC2 cluster PG-09 was reduced in response to infection in $CD11c^{\Delta raptor}$ compared with $CD11c^{WT}$ mice (Figures 3E and 3F). While PG-06 displayed overall high metabolic enzyme expression, it did not show an enhanced maturation compared with other clusters (Figure 3D), making it unlikely that the accumulation of this cDC1 cluster underpins the $CD8^+$ T cell phenotype in the $CD11c^{\Delta raptor}$ mice following Lm infection.

Since cross-presentation by DCs contributes to proper priming of $CD8^+$ T cell responses against Lm infection (Reinicke et al., 2009) and that autophagy, a process known to be enhanced by mTORC1 inhibition (Saxton and Sabatini, 2017), can promote cross-presentation (Mintern et al., 2015), we tested whether cross-presentation was enhanced in DCs lacking raptor. However, the capacity of raptor-deficient splenic cDC1s to cross-present soluble antigen, as assessed by their ability to present the H-2Kb-restricted $OVA_{257-264}$ short peptide (SIINFEKL) on MHC class I following exposure to a synthetic long peptide (SLP) variant that contains this epitope, was reduced (Figure 3G). Cross-presentation of cell-associated antigen, as assessed by their ability to induce $CD8^+$ T cell proliferation following stimulation with heat-killed Lm-OVA (Theisen et al., 2018), was also reduced in raptor-deficient splenic cDC1s, both in the presence and the absence of TLR stimulation (Figure 3H).

As rapamycin can promote BMDC longevity and sustain high costimulatory molecule expression after TLR stimulation (Amiel et al., 2012), we next assessed survival and maturation of splenic cDCs from $CD11c^{WT}$ and $CD11c^{\Delta raptor}$ mice after *ex vivo* TLR stimulation. However, no differences in survival (Figure S2B) or maturation (Figure S2C) were observed. Likewise, production of interleukin-12 (IL-12), a cytokine that increases IFN-γ production by $CD8^+$ T cells (Mashayekhi et al., 2011) and that is known to be sensitive to mTOR inhibition (Snyder and Amiel, 2018), was unaffected (Figure 3I). IL-10 production, which can limit $CD8^+$ T cell priming independent of IL-12 (Fu et al., 2015), was also unaffected (Figure 3J). More importantly, when mice were immunized with these cDC1s, no differences were observed in $CD8^+$ T cell-priming capacity (Figures 3K and 3L). Taken together, these data suggest that raptor deficiency in splenic cDC1s compromises MHC class I expression and cross-presentation,

Figure 2. $CD8^+$ T cell priming in response to listeria infection and host protection are intact in mice with raptor-deficient APCs

(A) On the top, a gating strategy for splenic T cell subsets. Frequencies and numbers of splenic T cells are enumerated on the bottom.

(B–E) $CD11c^{WT}$ and $CD11c^{\Delta raptor}$ mice were infected with 5×10^6 Lm-ΔActa-OVA intravenously (i.v.), and splenic T cell responses were analyzed 7 days later by flow cytometry.

(B) Total cell numbers in spleen.

(C) Frequencies and numbers of splenic $CD8^+$ T cell subsets as analyzed by flow cytometry. For representative histograms, see Figure S1B.

(D) Frequencies and numbers of OVA-specific $CD8^+$ T_{AE} cells based on K^bOVA-tetramer staining as analyzed by flow cytometry.

(E) Splenocytes were stimulated with SIINFEKL in the presence of Brefeldin A and analyzed for OVA-specific IFN-γ production by $CD8^+$ T_{AE} cells using flow cytometry.

(F) Mice were infected with 5×10^6 Lm-ΔActa-OVA by retro-orbital i.v. injection and challenged 21 days later with 5×10^4 Lm-OVA. The burden of LM-OVA in spleen and liver were determined on day 24.

Bars represent mean ± SEM of indicated data points from individual mice. Unpaired Student's t test (A), one-way ANOVA (B–E), and two-way ANOVA (F) were used to assess statistically significant differences. Data are from 2 experiments using 1–3 mice per group (A), 3 experiments using 1–4 mice per group (B–E), or 2 experiments using 5–7 mice per group (F).

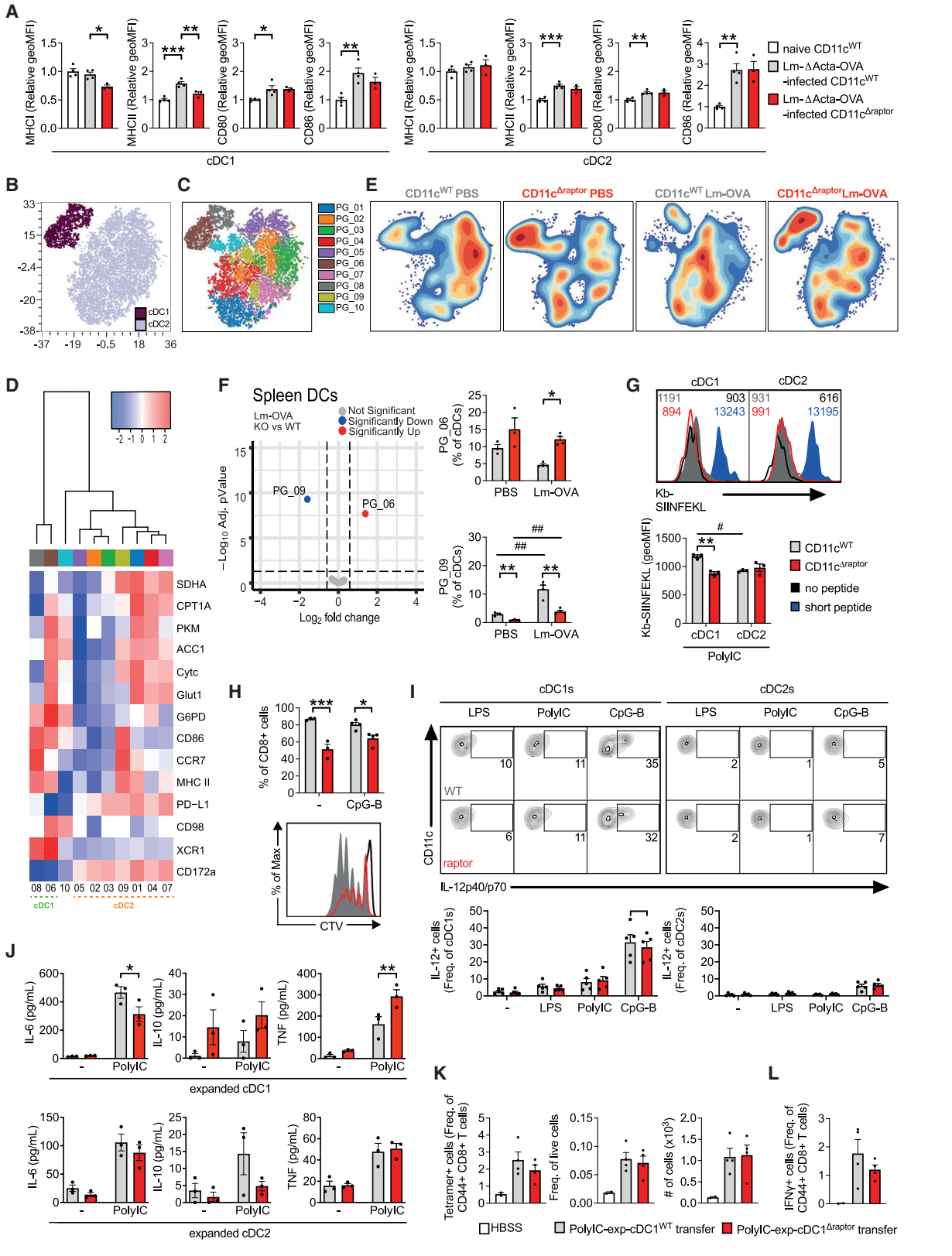

(legend on next page)

without significantly affecting their longevity, maturation duration, cytokine production, and CD8$^+$ T cell priming.

mTORC1 signaling supports maturation of migratory skin cDCs

As mTOR signaling impacts DC biology differently depending on the tissue DCs reside in (Sinclair et al., 2017), we extended our investigation to skin-draining lymph nodes (sdLNs) (Figure 4A). Steady-state phosphorylation of ribosomal protein S6 was reduced in raptor-deficient sdLN cDCs and LCs (Figures 4B and S3A). Under steady-state conditions, both the frequency and number of migratory DCs (migDCs) were higher in sdLNs from CD11c$^{\Delta raptor}$ mice than in sdLNs from CD11c^{WT} mice (Figures 4A and 4C), suggesting that loss of raptor might potentiate their migration. In contrast, and in line with work showing that LCs depend on mTORC1 signaling for their survival (Kellersch and Brocker, 2013), we found that deletion of raptor in CD11c-expressing cells decreased LC frequency within the migratory APC (migAPC) gate (Figures 4A and 4C). However, due to the overall increased migAPC pool size (Figure 4C), the total number of LCs in sdLNs was not different between CD11c^{WT} and CD11c$^{\Delta raptor}$ mice (Figure 4C). Resident DC (resDC) homeostasis was unchanged (Figures 4A and 4C). Like splenic cDC1s, skin migDC1s showed high 2-NBDG uptake, mitochondrial membrane potential, and mass relative to other APCs (Figures 4D, 4E, and S3B). However, none of these parameters were affected at steady state by loss of raptor in any of the DC subsets (Figures 4D and 4E). To more fully characterize possible changes in cellular metabolism, we performed Met-flow analysis (Figure 1F). This revealed that sdLN cDC1s generally display higher expression of metabolic enzymes than cDC2s and pDCs. However, expression of acetyl-coenzyme A (CoA) carboxylase 1 (ACC1), a cytosolic enzyme involved in fatty acid synthesis, was selectively high in LCs, and its expression was dependent on raptor in cDC1s, cDC2s, and LCs (Figure 4F). In addition, CPT1a and respiratory chain complex cytochrome C (CytC) were inversely affected by loss of raptor in LCs; ACC1 expression decreased, while CytC expression increased. These metabolic changes were accompanied by impaired maturation of migDC1s and migDC2s (Figures 4G and S3C). On the other hand, LC maturation was not affected by loss of raptor (Figure 4G). Together, these data reveal that loss of mTORC1 signaling affects steady-state metabolism and maturation of migratory skin APC subsets to various degrees, with the strongest effects on LC metabolism and cDC1 maturation.

mTORC1 signaling in CD11c-expressing cells limits CD8$^+$ T cell priming following s.c. immunization

Because raptor-deficient sdLN migAPCs displayed an overall weaker maturation profile, we first investigated if the T cell compartment in sdLNs from CD11c$^{\Delta raptor}$ mice was changed under steady-state conditions. Corresponding with the data from the circulation, the frequency of effector CD8$^+$ T cells was reduced in sdLNs from naïve CD11c$^{\Delta raptor}$ mice (Figure 5A). Since we found raptor-deficient cDC2s in sdLNs to have reduced MHC class II expression (Figure 4F), which has been implicated in favoring the priming of CD4$^+$ T helper 2 (Th2) cells *in vivo* (van Panhuys et al., 2014), we evaluated their capacity to prime Th2 responses. In addition, pharmacological inhibition of mTORC1 in human monocyte-derived DCs has been shown to enhance their Th2-priming capacity *in vitro* (Hussaarts et al., 2013). However, loss of raptor in CD11c-expressing cells did not affect the secretion of type 2 cytokines by sdLN cells after footpad injection with a soluble antigen extract of *Schistosoma mansoni* eggs (Figure 5B) nor the production of type 2 cytokines by CD44$^+$CD4$^+$ cells in the liver and draining hepatic LNs during systemic *S. mansoni* infection (Figure S4). Together, these data suggest that mTORC1 signaling in CD11c-expressing cells is

Figure 3. mTORC1 signaling is required for cross-presentation but dispensable for longevity, maturation duration, and cytokine production of splenic cDCs

(A) CD11c^{WT} and CD11c$^{\Delta raptor}$ mice were infected with 2.5 × 10^5 Lm-ΔActA-OVA by retro-orbital i.v. injection, and splenic cDC surface protein expression of indicated surface markers was analyzed 1 day later by flow cytometry.

(B) Unbiased opt-SNE analysis of cDC population cDC1s and cDC2s are indicated.

(C) Phenograph clustering performed on splenic cDCs using metabolic and lineage markers.

(D) Heatmap displaying expression of metabolic, activation, and lineage markers from clusters identified in (C).

(E) Contour plots overlaid on opt-SNE analysis as shown in (B) displaying distribution of cells for CD11c^{WT} and CD11c$^{\Delta raptor}$ mice challenged with PBS or 2.5 × 10^5 Lm-OVA for 1 day.

(F) Left: volcano plot displaying the clusters as displayed in (C) and (D) with significant differences in frequency between Lm-OVA-challenged CD11c^{WT} and CD11c$^{\Delta raptor}$ mice. Right: graphics displaying frequencies of cDC1 and cDC2 clusters 06 and 09.

(G) Flow cytometry-based analysis of cross-presentation in splenic cDCs from CD11c^{WT} mice in gray, CD11c$^{\Delta raptor}$ mice, a no-antigen negative control, in black, and a SIINFEKL-positive control in blue.

(H) Sort-purified splenic cDC1s from CD11c^{WT}and CD11c$^{\Delta raptor}$ mice were cultured for 3 days with CTV-labeled OT-I T cells in the presence of 1 × 10^7 heat-killed Lm-OVA, and T cell proliferation was assessed by CTV dilution.

(I) Splenocytes from naïve WT and CD11c$^{\Delta raptor}$ mice were stimulated with indicated TLR ligands in the presence of Brefeldin A and analyzed for production of IL-12p40/p70 by splenic cDCs using flow cytometry.

(J–L) *In vivo* Flt3L-expanded splenic cDC1s and cDC2s were sorted using a flow cytometer and (J) put into culture with or without polyIC, after which supernatants were analyzed for indicated cytokines by cytokine bead array or (K and L) conditioned with OVA and polyIC for 5 h *ex vivo* before transfer into recipient mice by footpad injection.

(K) Frequencies and numbers of OVA-specific CD8$^+$ T_{AE} cells based on K^{b}OVA-tetramer staining as analyzed by flow cytometry.

(L) Splenocytes were stimulated with SIINFEKL in the presence of Brefeldin A and analyzed for OVA-specific IFN-γ production by CD8$^+$ T_{AE} cells using flow cytometry. Bars represent mean ± SEM of indicated data points from individual mice. One-way ANOVA (A, K, and L), two-way ANOVA (F–H), and two-way ANOVA for repeated measures (I–J) were used to assess statistically significant differences. Data are from 1 experiment using 4 mice per group (A–F), 1 experiment using 3 mice per group (G), representative of 1 out of 2 experiments with 3–4 mice per group (H), 5 experiments using 1 mouse per group (I), 1 experiment using 3 mice per group (J), or 1 experiment using 2–4 mice per group (K and L).

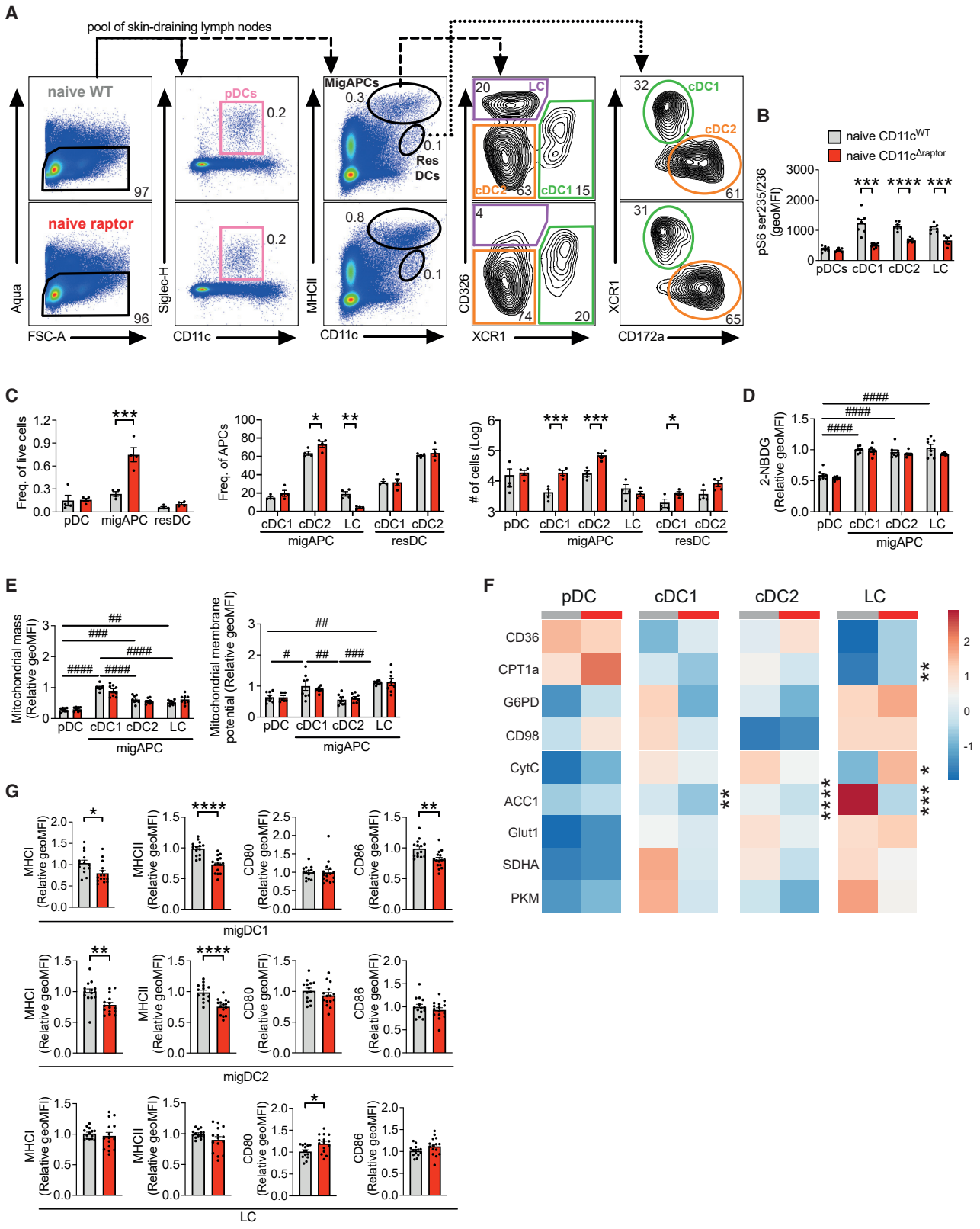

(legend continued on next page)

not important for the generation of Th2 cell responses. Finally, we assessed whether the reduced activation profile of sdLN migDC1s in CD11c$^{\Delta raptor}$ mice would affect CD8$^+$ T cell priming following s.c. immunization. Mice were immunized with the TLR9 ligand CpG-B in combination with a synthetic 43-mer-long peptide from the human papillomavirus (HPV) E7 protein that contains the immunodominant and H-2Db-restricted epitope RAHYNIVTF (E7-SLP), a combination that predominantly activates cDC1s and requires cross-presentation for priming of CD8$^+$ T cells (Maynard et al., 2019). Of note, this peptide does not contain any I-Ab restricted CD4$^+$ T cell epitopes, which allows for assessing CD8$^+$ T cell priming without CD4$^+$ T cell help. This resulted in enhanced frequencies and numbers of E7-specific CD8$^+$ T cells in sdLNs from CD11c$^{\Delta raptor}$ mice compared with sdLNs from their CD11c^{WT} littermates (Figure 5C), as well as enhanced IFN-γ production by these cells after *ex vivo* antigen-specific restimulation (Figure 5D). These effects were independent of antigen or TLR stimulus, as enhanced IFN-γ production by CD8$^+$ T cells and trends toward higher frequencies and numbers of antigen-specific CD8$^+$ T cells were also observed in CD11c$^{\Delta raptor}$ mice after immunization with CpG-B with full-length OVA (Figures 5E and 5F) or polyIC with E7-SLP (Figure 5G).

mTORC1 signaling constrains activation of LCs and a subpopulation of EpCAM$^+$ cDC1s in response to s.c. immunization

To find a mechanistic basis for the enhanced IFN-γ production by CD8$^+$ T cells in CD11c$^{\Delta raptor}$ mice after s.c. immunization, we assessed how loss of raptor affected metabolism, maturation, cytokine production, and migration of sdLN migAPCs in response to these immunizations. TLR stimulation resulted in increased S6 phosphorylation in wild-type (WT) cDC2s and LCs and remained low in all migAPC subsets from CD11c$^{\Delta raptor}$ mice (Figure S5A). After TLR stimulation, all raptor-deficient migAPC subsets showed increased mitochondrial membrane potential (Figure 6A) as well as restoration of MHC class I surface expression (Figure 6B). Raptor-deficient LCs were the only subset to additionally show enhanced costimulatory molecule expression (Figures 6B and S5B–S5D) and IL-12 production (Figures 6C and S5E). To better understand the interaction between loss of raptor and immunization, Metflow data (Figure 1E) were subjected to dimensional reduction and unsupervised clustering. We could identify cDC1s, cDC2s, and LCs (Figure 6D) that could be further split into several phenotypically distinct clusters (Figures 6E and 6F). Frequencies of several clusters were changed as a consequence of loss of raptor in CD11c-expressing cells and/or immunization (Figure 6G). Among those, LC clusters PG-06 and PG-10 were most strongly modulated by raptor deletion (Figure 6H). PG-10, abundant in WT mice and characterized by high ACC1 and low PD-L1 expression, was largely replaced by PG-06, which instead displayed low ACC1 but high CPT1a and PD-L1 expression (Figures 6F, 6H, and S6). These pronounced changes in the phenotype of raptor-deficient LCs prompted us to explore their role in the enhanced CD8$^+$ T cell response of immunized CD11c$^{\Delta raptor}$ mice. We first evaluated LC migratory capacity from the skin to the sdLNs in a fluorescein isothiocyanate (FITC)$^+$ skin-painting model, but no differences were found 24 and 72 h after painting (Figure 6I). We then sorted LCs from the sdLNs of CpG-B + OVA-immunized mice and cocultured them with naïve OT1 cells, but proliferation and IFN-γ production were unaltered by loss of raptor in LCs (Figures 6J and 6K). This suggests that despite the more inflammatory profile of LCs from CD11c$^{\Delta raptor}$ mice, they do not play a prominent role in the potentiated CD8$^+$ T cell response in these mice.

The unsupervised clustering additionally revealed an EpCAM$^+$ cluster within the total cDC1 population (PG-09; Figure 6H) that selectively increased in frequency following immunization of CD11c$^{\Delta raptor}$ mice (Figures 7A and 7B). Notably, this EpCAM$^+$ cDC1 subpopulation from CD11c$^{\Delta raptor}$ mice was characterized by high expression of glycolytic and mitochondrial markers relative to other cDC1 clusters (Figure 6F) and, unlike EpCAM$^-$ cDC1s, maintained its activation profile, or even increased it in the case of CD80, after immunization (Figures 7C–7E). Due to the rarity of these cells, we were not able to sort them to interrogate their T cell-priming capacity *ex vivo*. We therefore instead quantified the frequency of physically interacting DC-T cell pairs by flow cytometry following immunization (Giladi et al., 2020) (Figure S7) as a measure of active T cell priming by DCs *in situ*. This specifically revealed a significantly increased frequency of EpCAM$^+$ cDC1-CD8$^+$ T cell pairs in sdLNs from CD11c$^{\Delta raptor}$ mice compared with CD11c^{WT} mice following immunization (Figure 7F). Taken together, these alterations in the cDC1 compartment may help to explain the enhanced CD8$^+$ T cell response in CD11c$^{\Delta raptor}$ mice after s.c. immunization.

Figure 4. mTORC1 signaling is required for maintenance of MHC expression by migratory skin cDCs and of ACC1 expression by cDCs and LCs

(A) Flow gating strategy for LCs and DC subsets in skin-draining lymph nodes (sdLNs).

(B) Flow-cytometry-based analysis of S6 phosphorylation on serine 235/236 in pDCs, migcDC1s, migcDC2s, and LCs from sdLNs out of CD11c^{WT} and CD11c$^{\Delta raptor}$ mice. Representative histograms are in Figure S3A. sdLNs were a pool of brachial, axillary, and inguinal LNs.

(C) Frequencies and numbers of LC and DC subsets in sdLNs as gated in (A) are enumerated. Migratory DCs are migAPCs minus LCs in the left panel.

(D) Flow-cytometry-based analysis of overall metabolic pathway engagement by sdLN LCs and cDCs using the fluorescent glucose analog 2-NBDG.

(E) Flow-cytometry-based analysis of mitochondrial mass and mitochondrial membrane potential in sdLNs of LC and cDC subsets using MitoTracker Green and TMRM, respectively.

(F) Heatmap displaying the expression of metabolic targets in sdLN pDC, LC, and migDC subsets. Expression levels for each marker are shown relative to all DC subsets.

(G) Flow-cytometry-based analysis of surface expression of indicated markers of sdLN migcDC1s, migcDC2s, and LCs.

Bars represent mean ± SEM of indicated data points from individual mice. Unpaired Student's t test (A, C, F, and G) and two-way ANOVA (D and E) were used to assess statistically significant differences. Data are from 1 out of 2 representative experiments using 4 mice per group (B, C, and F) or relative geoMFI from a pool of 2 independent experiments (D, E, and G).

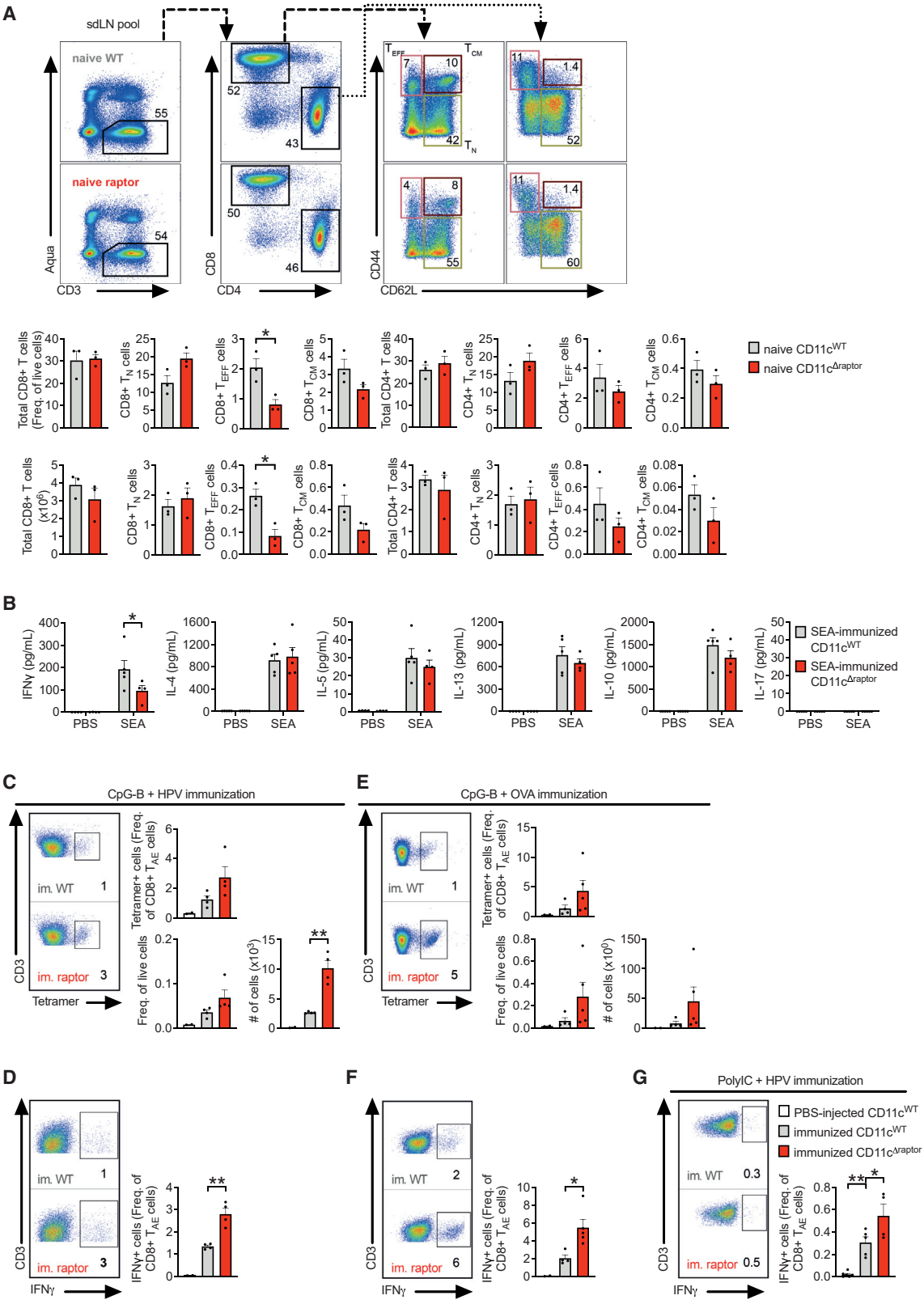

(legend on next page)

DISCUSSION

In the present study, we aimed to determine how mTORC1 regulates DC metabolism and their T cell priming capacity *in vivo*. We show that the metabolic and immunological phenotype of professional APCs are differently affected by loss of mTORC1 signaling, depending on their origin and location. Apart from compromised MHC class I expression, deletion of raptor minimally affected splenic cDC phenotypes. On the other hand, loss of raptor resulted in a strongly reduced maturation profile of migAPCs in sdLNs, while conversely increasing their abundance, with the notable exception of LCs and an EpCAM$^+$ cDC1 subpopulation. These latter findings were associated with a potentiated ability of CD11c$^{\Delta raptor}$ mice to mount CD8$^+$ T cell responses following s.c. immunization. Together, these data highlight distinct functional effects of mTORC1 signaling on different APC subsets and suggest that mTORC1 acts as a negative regulator of CD8$^+$ T cell priming in dermal cDC1s.

In line with a recent study (Du et al., 2018), we found that splenic cDC1s display higher uptake of the fluorescent glucose analog 2-NBDG, mitochondrial mass, and membrane potential than splenic cDC2s. We here report that the expression of several rate-limiting enzymes in key metabolic pathways are also higher in splenic cDC1s than cDC2s and that this feature of a generally metabolically more active cDC1s extends to skin migDC1s, as they had higher mitochondrial mass, mitochondrial membrane potential, and expression of several metabolic enzymes than migDC2s. Consistent with a well-described role for mTORC1 signaling in supporting glycolysis (Weichhart et al., 2015), 2-NBDG uptake by splenic cDC1s was reduced following loss of mTORC1 signaling, although this appeared not to be mirrored by reduced Glut1 or PKM expression in these cells. In fact, loss of raptor had little impact on the expression of any of the analyzed metabolic enzymes in splenic cDCs under steady state. In contrast, 2-NBDG uptake by sdLN APC subsets was not affected by loss of raptor, while ACC1 expression was strongly reduced in all migAPCs. How mTORC1 differentially affects the metabolism of DCs at different locations is currently unclear but is likely to be influenced by local nutrient and growth factor availability, which are both important determinants of mTORC1 activity.

Moreover, we found that raptor-deficient cDCs show a consistent reduction in MHC class I surface expression during steady state. Lower baseline MHC class I expression on raptor-deficient cDCs did not, however, translate into an impaired ability of CD11c$^{\Delta raptor}$ mice to mount CD8$^+$ T cell responses to foreign antigens. This was apparent during both systemic (listeria infection) and local (s.c. immunization with TLR ligands) immunological challenge or after adoptive transfer. In fact, antigen-specific CD8$^+$ T cell responses in CD11c$^{\Delta raptor}$ mice were even potentiated following s.c. immunization. While our data suggest that the latter observation—as discussed in more detail below—may be driven by a small subpopulation of highly active cDC1s, the intact CD8$^+$ T cell priming after listeria infection is likely to have a different basis. Although Lm primarily infects splenic macrophages and liver Kupffer cells, cDC1s are also directly infected and serve as a critical entry point to establish infection (Edelson et al., 2011). Following internalization, the bacteria can escape from phagosomes and access the host cytosol for replication. Hence, listeria-derived antigens from both exogenous/vacuolar and cytosolic origin can be presented in MHC class I, via cross- and direct presentation, respectively (Reinicke et al., 2009; Villanueva et al., 1995). Our observation that cross-presentation is reduced in raptor-deficient splenic cDC1s might indicate that, instead, presentation of cytosolic listeria-derived antigens is enhanced. mTORC1 inhibition is well known to promote autophagy, which, by breaking down intracellular bacteria, can directly serve as a host protective mechanism (Jagannath et al., 2009; Riebisch et al., 2021) as well as by facilitating the generation of peptides for presentation on MHC class I (Fiegl et al., 2013). Further studies are required to determine whether enhanced presentation of autophagy-derived antigens can compensate for lower MHC class I expression and explain the uncompromised ability of CD11c$^{\Delta raptor}$ mice to mount antigen-specific CD8$^+$ T cell responses following listeria infection.

Several aspects of cDC biology at the population level—including longevity, the magnitude and duration of expression of costimulatory markers, and cytokine expression and

Figure 5. mTORC1 signaling in CD11c-expressing cells limits CD8+ T cell priming following s.c. immunization but not Th2 polarization

(A) On the top, a gating strategy for T cell subsets in sdLNs, as shown in Figure 2A. Frequencies and numbers of splenic T cells are enumerated on the bottom.

(B) CD11c^{WT} and CD11c$^{\Delta raptor}$ mice were immunized with *S. mansoni* soluble egg antigens (SEAs) by s.c. footpad injection, draining popLNs were collected 7 days later, and supernatants from *ex vivo* restimulated cells were analyzed for indicated cytokines by cytokine bead array.

(C and D) Mice were immunized with HPV SLP and 25 μg CpG-B by s.c. tailbase injection, and T cell responses in draining inguinal lymph nodes (ingLNs) were analyzed 7 days later by flow cytometry.

(C) Representative histograms, frequencies, and numbers of E7-specific CD8$^+$ T_{AE} cells based on D^{b}E7-tetramer staining as analyzed by flow cytometry.

(D) IngLN cells were stimulated with E7-SLP in the presence of Brefeldin A and analyzed for HPV-specific IFN-γ production by CD8$^+$ T_{AE} cells using flow cytometry.

(E and F) Mice were immunized with OVA and 25 μg CpG-B by s.c. footpad injection, and T cell responses in draining popLNs were analyzed 7 days later by flow cytometry.

(E) Representative histograms, frequencies, and numbers of OVA-specific CD8$^+$ T_{AE} cells based on K^{b}OVA-tetramer staining as analyzed by flow cytometry.

(F) PopLN cells were stimulated with SIINFEKL in the presence of Brefeldin A and analyzed for OVA-specific IFN-γ production by CD8$^+$ T_{AE} cells using flow cytometry.

(G) Mice were immunized with HPV peptide and polyIC by s.c. tailbase injection, and T cell responses in draining ingLNs were analyzed 7 days later by flow cytometry. IngLN cells were stimulated with E7-SLP in the presence of Brefeldin A and analyzed for E7-specific IFN-γ production by CD8$^+$ T_{AE} cells using flow cytometry.

Bars represent mean ± SEM of indicated datapoints from individual mice. Unpaired Student's t test (A), two-way ANOVA (B), and one-way ANOVA (C–G) were used to assess statistically significant differences. Data are from 1 experiment using 3 mice per group (A), 1 experiment using 4–5 mice per group (B), 1 experiment using 2–4 mice per group (C and D), 1 experiment using 2–5 mice per group (E and F), or 1 experiment using 2 lymph nodes from 2–3 mice per group (G).

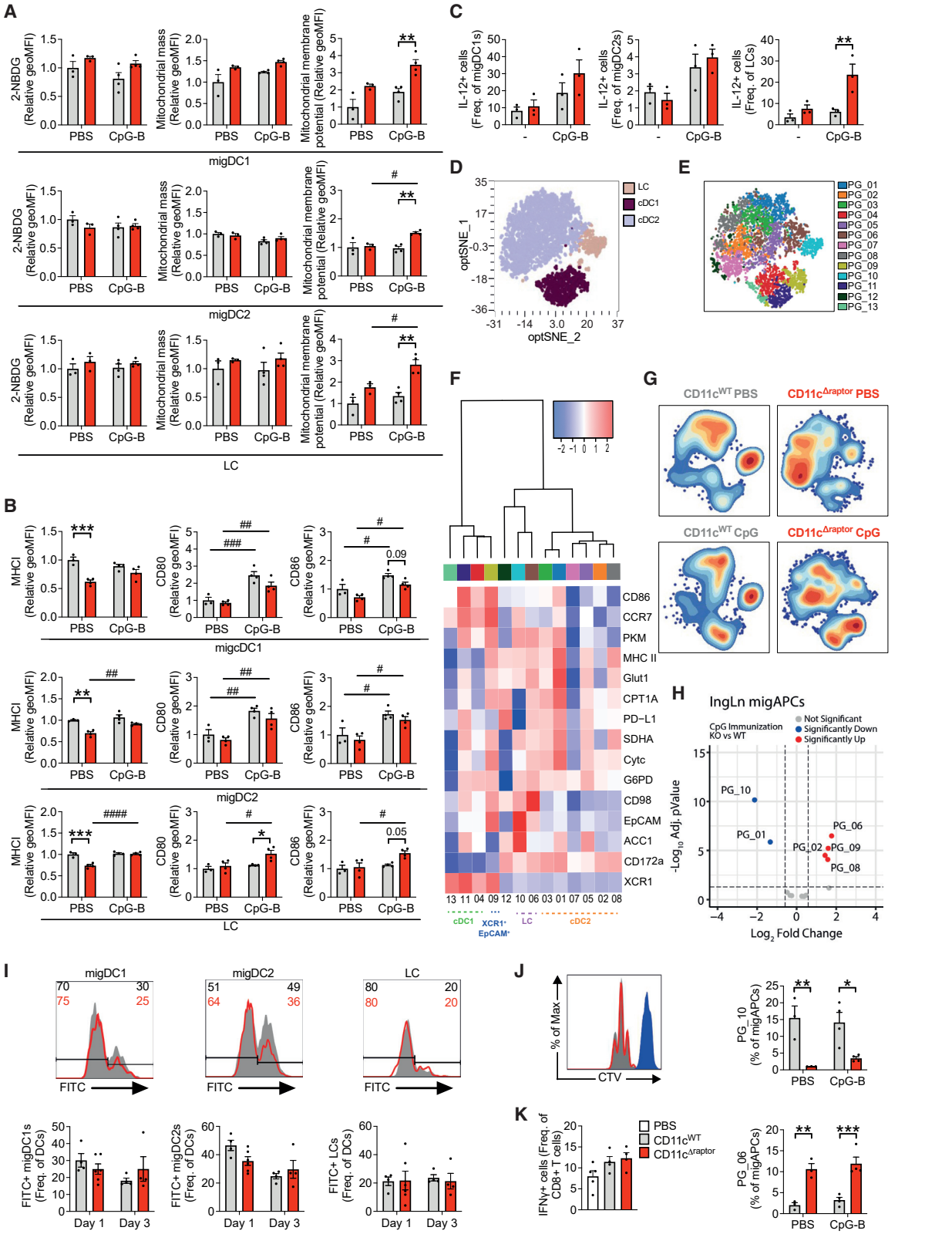

(legend on next page)

migration—that could potentially explain the differences in CD8$^+$ T cell phenotype between CD11c^{WT} and CD11c$^{\Delta raptor}$ mice were not substantially different between TLR-stimulated cDCs from both strains, both *in vivo* and *ex vivo*. This shows that the phenotype of increased survival and duration of costimulatory molecule expression by TLR-activated granulocyte macrophage-colony-stimulating factor (GM-CSF)-induced DCs (GMDCs) after treatment with rapamycin, resulting in an enhanced CD8$^+$ T cell-priming capacity following adoptive transfer *in vivo* (Amiel et al., 2012; Jagannath and Bakhru, 2012; Jagannath et al., 2009), does not translate to cDCs. This likely stems from the fact that TLR-activated GMDCs, in contrast to cDCs, express inducible NO synthase (iNOS) to produce NO in an mTORC1-dependent manner (Thwe and Amiel, 2018), which has been shown to poison mitochondrial respiration in an autocrine manner and thereby compromise longevity of GMDCs (Everts et al., 2012). In search of an alternative explanation for the potentiated antigen-specific CD8$^+$ T cell response following s.c. immunization in CD11c$^{\Delta raptor}$ mice, we explored the role of LCs in this phenotype. In contrast to cDCs, loss of raptor augmented the activation of LCs, as reflected by increased CD80, CD86, and IL-12 expression and maintenance of MHC class I expression following immunization with TLR ligands. In addition, only LC frequencies, and not total numbers, were significantly reduced in sdLNs, which is largely consistent with earlier studies (Kellersch and Brocker, 2013). Moreover, we found that among the migAPCs, LCs showed the most significantly changed metabolic and immunological phenotype after raptor loss. Metabolically, the increased CPT1a expression at the expense of ACC1, together with increased mitochondrial membrane potential, indicates a shift towards catabolism. This metabolic state has both been linked to supporting tolerogenic as well as immunogenic properties of DCs (Malinarich et al., 2015; Qiu et al., 2019; Sun et al., 2019). Whether there is a causal link between catabolic metabolism and immunogenicity in raptor-deficient LCs remains subject for further study.

Ex vivo cocultures, however, did not reveal an enhanced CD8$^+$ T cell priming capacity of raptor-deficient LCs, suggesting that these phenotypic differences in the total LC population are not sufficient to explain the potentiated CD8$^+$ T cell priming in CD11c$^{\Delta raptor}$ mice. This would be largely consistent with studies showing that murine LCs are poor cross-presenters compared with murine cDC1s and human LCs (Artyomov et al., 2015; Kaplan, 2017) and are dispensable for the generation of CD8$^+$ T cell responses to various infections (Allan et al., 2003; Igyártó et al., 2011; Kaplan, 2017; Seneschal et al., 2014). However, this does not exclude the possibility that increased IL-12 production by raptor-deficient LCs—analogous to what has been shown for IL-12-producing monocyte-derived DCs (Hilligan et al., 2020)—may assist cDCs in supporting or enhancing generation of cellular type 1 immune responses in CD11c$^{\Delta raptor}$ mice.

Finally, we identified a subpopulation of cDC1s, characterized by EpCAM expression, that selectively accumulated in sdLNs of immunized CD11c$^{\Delta raptor}$ mice. This population was characterized by higher metabolic enzyme and costimulatory molecule expression compared with that same subset from CD11c^{WT} mice and higher MHC class I expression than the EpCAM$^-$ cDC1 population from these mice. Importantly, corresponding with this highly immunogenic phenotype, this population physically interacted more frequently with CD8$^+$ T cells in sdLNs of immunized CD11c$^{\Delta raptor}$ mice. EpCAM$^+$ cDC1s have recently been identified in the context of cutaneous bacterial infections, where they were found to play a key innate role by recruiting neutrophils through production of vascular endothelial growth factor α (VEGFα) (Janela et al., 2019). However, in this study, their role in CD8$^+$ T cell priming was not assessed. Now, our findings would indicate that this population can also have an important role in regulating adaptive immune responses. Interestingly, VEGFα expression by EpCAM$^+$ cDC1s was found to depend on hypoxia inducible factor 1α (HIF1α), a transcription factor known to promote glycolysis. In line with this, we show here

Figure 6. mTORC1 signaling supports activation of migratory skin cDCs but constrains activation of Langerhans cells in response to subcutaneous immunization

(A–H) CD11c^{WT} and CD11c$^{\Delta raptor}$ mice were immunized with 25 μg CpG-B by s.c. tailbase injection, and draining ingLNs were analyzed 24 h later by flow cytometry.

(A) sdLN LC and migDC subsets were analyzed by flow cytometry using the fluorescent glucose analog 2-NBDG, MitoTracker Deep Red, and TMRM to evaluate glucose uptake, the mitochondrial mass, and mitochondrial membrane potential, respectively.

(B) Flow-cytometry-based analysis of surface expression of indicated markers by migDC1s, migDC2s, and LCs.

(C) IngLN cells from naive WT and CD11c$^{\Delta raptor}$ mice were *ex vivo* stimulated with 5 μg/mL CpG-B in the presence of Brefeldin A and analyzed for production of IL-12p40/p70 by indicated APCs using flow cytometry.

(D) Unbiased opt-SNE analysis of migAPC population in which migcDC1s, migcDC2s, and LCs are indicated.

(E) Phenograph clustering performed on migAPCs using metabolic and lineage markers.

(F) Heatmap displaying expression of metabolic, activation, and lineage markers from clusters identified in (E).

(G) Contour plots overlaid on opt-SNE analysis as shown in (D) displaying distribution of cells for CD11c^{WT} and CD11c$^{\Delta raptor}$ mice immunized with either PBS or CpG-B.

(H) Top: Volcano plot displaying the clusters as displayed in (E) and (F) with significant differences in frequency between CpG-B-immunized CD11c^{WT} and CD11c$^{\Delta raptor}$ mice. Bottom: graphics displaying frequencies of LC clusters 10 and 06.

(I) Mice were painted on their flank with inflammatory FITC, and frequencies of FITC$^+$ migcDC1s, migcDC2s, and LCs were analyzed on the indicated days by flow cytometry.

(J and K) LCs were flow sorted and cocultured with CTV-labeled OT-I T cells (either in the presence or absence [blue] of OT-I peptide) to evaluate the (J) proliferation and (K) IFN-γ secretion by OT-I T cells 3 days later.

Bars represent mean ± SEM of indicated data points from individual mice. Two-way ANOVA (Aand H), two-way ANOVA for repeated measures (C), and one-way ANOVA (K) were used to assess statistically significant differences. Data are from 1 experiment using 2 lymph nodes from 2 mice per group (A), 3 experiments using 1 mouse per group (B), representative of 1 out of 2 independent experiments using 4–6 mice per group (C), 1 experiment using 3–4 mice per group (D), representative of 1 out 2 independent experiments using 3–4 mice per group (E–I), and 1 experiment using pooled sorted LCs from 4 CpG-B-immunized mice. (A and B) Data represent normalized geoMFI relative to PBS-injected CD11c^{WT} group.

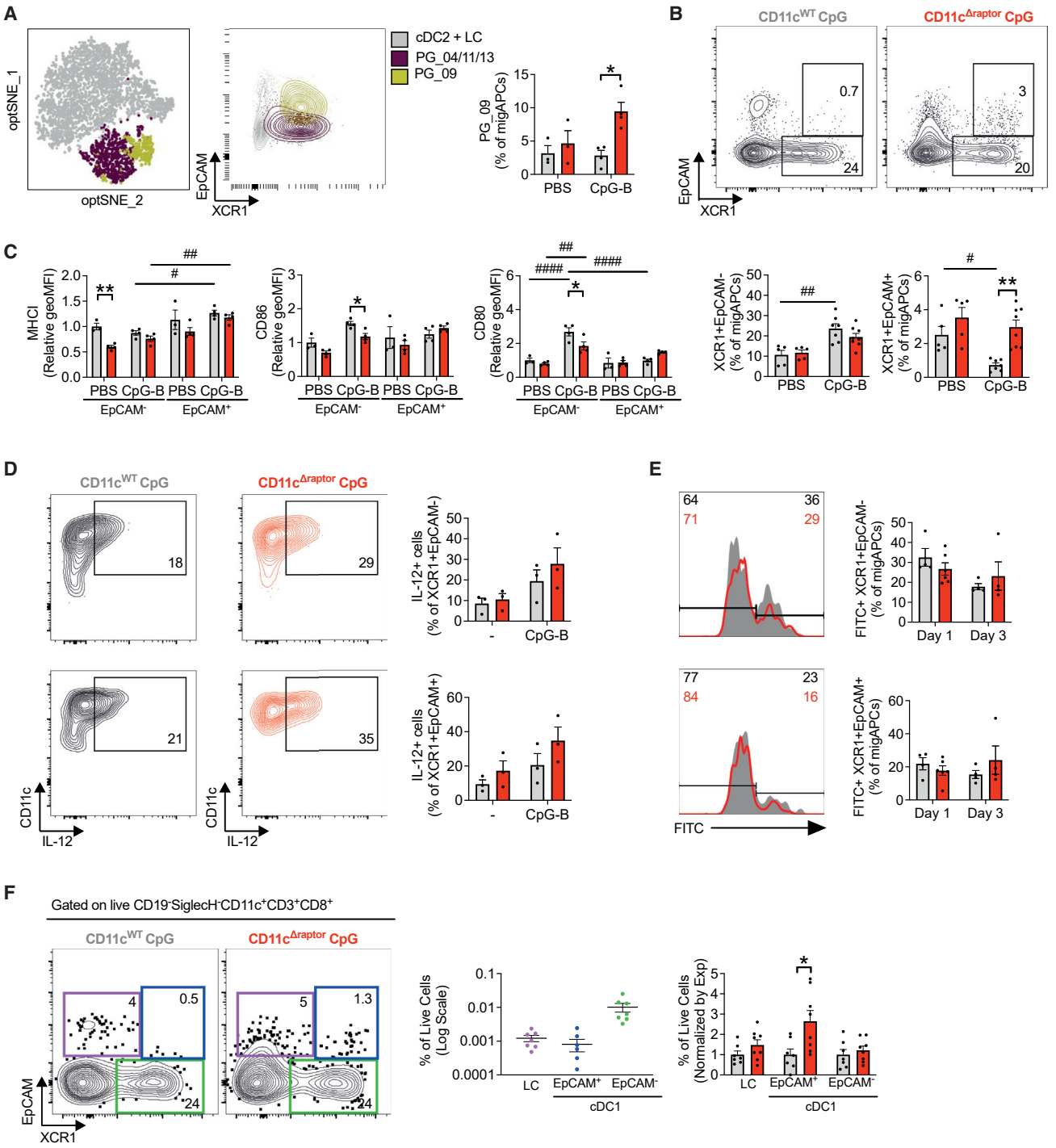

Figure 7. Loss of mTORC1 signaling results in accumulation of a subpopulation of immunogenic EpCAM$^+$cDC1s with increased potential to interact with CD8$^+$ T cells following immunization

(A–C) Mice were immunized with 25 μg CpG-B and 50 μg OVA by s.c. tailbase injection, and draining ingLNs were analyzed 24 h later by flow cytometry.

(A) opt-SNE analysis (top left panel) in which cDC1 cluster PG_09 and remaining cDC1 clusters (PG04_PG11_PG13) are indicated. Expression patterns of XCR1 and CD326 (EpCAM) by these clusters are shown in the middle plot. Frequency of PG_09 within DC gate is shown on right.

(B) Frequency of EpCAM$^-$ and EpCAM$^+$ cDC1s in naïve and CpG-B-immunized mice based on manual gating as shown in top panels.

(C) Maturation status of EpCAM$^+$ and EpCAM$^-$ cDC1s in naïve and CpG-B-immunized mice.

(D) IngLN cells from naïve CD11c^{WT} and CD11c$^{\Delta raptor}$ mice were stimulated *ex vivo* with CpG-B and analyzed for production of IL-12p40/p70 by EpCAM$^+$ and EpCAM$^-$ cDC1s using flow cytometry.

(legend continued on next page)

that EpCAM$^+$ cDC1s have higher 2-NBDG uptake and glycolytic enzyme expression than EpCAM$^-$ cDC1s. Interestingly, we have previously shown this metabolic profile to be required for DCs to optimally prime CD8$^+$ T cell responses (Everts et al., 2014). Hence, in the light of the well-known key role of cDC1s in priming CD8$^+$ T cell responses (Hildner et al., 2008), these findings provide support for an important role for EpCAM$^+$ cDC1s, possibly in conjunction with LC-derived IL-12, in underpinning the enhanced CD8$^+$ T cell priming observed in CD11c$^{\Delta raptor}$ mice following s.c. immunization.

In conclusion, our observations highlight that pharmacological inhibition of mTORC1 may be a viable means to boost cellular immunity following vaccination. Interestingly, since LCs have also been reported to promote CD4$^+$ T follicular helper cell differentiation, germinal center formation, and humoral responses in a variety of settings (Bouteau et al., 2019; Levin et al., 2017; Marschall et al., 2020; Yao et al., 2015; Zimara et al., 2014), not only cellular, but also humoral, immune responses may benefit from local mTORC1 inhibition in response to vaccination and clearly warrant further study. In summary, our data provide evidence for distinct effects of mTORC1 signaling on the metabolic and immunological phenotype and CD8$^+$ T cell-priming function of different APC subsets, with selectively an inhibitory role for mTORC1 in these processes in LCs and a subpopulation of cDC1s, which may have implications for vaccination practices.

Limitations of the study

Although DCs are the primary cell type expressing CD11c, it is not limited to these cells. Therefore, we cannot formally rule out the possibility that some of the observed effects in the CD8$^+$ T cell compartment in CD11c$^{\Delta raptor}$ mice are a consequence of changes in CD11c-expressing cells other than DCs. In addition, due to the low frequency of EpCAM$^+$ cDC1s, we were not able to functionally test the CD8$^+$ T cell-priming ability of these cells. In this context, LC-specific hLangerin-cre and cDC1-specific XCR1-cre strains can be valuable tools to further elucidate the link between mTORC1 signaling in these cells and CD8$^+$ T cell priming *in vivo*.

STAR★METHODS

Detailed methods are provided in the online version of this paper and include the following:

SUPPLEMENTAL INFORMATION

Supplemental information can be found online at https://doi.org/10.1016/j.celrep.2022.111032.

ACKNOWLEDGMENTS

This work was supported by an LUMC fellowship awarded to B.E.

AUTHOR CONTRIBUTIONS

L.R.P., T.A.P., F.O., L.V.N., A.O.-F., A.J.v.d.H., G.A.H., H.J.P.v.d.Z., and B.E. performed experiments. L.R.P., T.A.P., and B.E. analyzed experiments. L.R.P., T.A.P., R.A., and B.E. designed experiments. B.E. conceived and supervised the study and wrote the manuscript together with L.R.P. and T.A.P.

DECLARATION OF INTERESTS

The authors declare no competing interests.

Received: May 27, 2021
Revised: April 21, 2022
Accepted: June 13, 2022
Published: July 5, 2022

REFERENCES

Ahl, P.J., Hopkins, R.A., Xiang, W.W., Au, B., Kaliaperumal, N., Fairhurst, A.M., Connolly, J.E., and Au, B. (2020). Met-Flow, a strategy for single-cell metabolic analysis highlights dynamic changes in immune subpopulations. Commun. Biol. *3*, 305. https://doi.org/10.1038/s42003-020-1027-9.

Allan, R.S., Smith, C.M., Belz, G.T., van Lint, A.L., Wakim, L.M., Heath, W.R., and Carbone, F.R. (2003). Epidermal viral immunity induced by CD8α^+

(E) Frequency of FITC$^+$ EpCAM$^+$ and EpCAM$^-$ cDC1s was analyzed in ingLNs on the indicated days by flow cytometry following FITC painting.
(F) DC-T cell interactions were analyzed by flow cytometry by gating on CD19$^-$SiglecH$^-$CD3$^+$CD8$^+$CD11c$^+$ cells without exclusion of doublets, followed by additional gating based on XCR1 and CD326 expression (left). Frequencies of CD8$^+$T cell-APC subset doublets from immunized CD11c^{WT} mice are quantified (middle plot) and shown as normalized data compared with data from immunized CD11c$^{\Delta raptor}$ mice (right plot).
Bars represent mean ± SEM of indicated datapoints from individual mice. Unpaired Student's t test (F) and two-way ANOVA (A–E) were used to assess statistically significant differences. Data are from of 1 representative out of 2 independent experiments using 4–6 mice per group (A and E), 2 experiments using 3–4 mice per group (B and F), and 1 experiment using 2 lymph nodes from 2 mice per group (C) and 3 mice per group (D).

dendritic cells but not by Langerhans cells. Science *301*, 1925–1928. https://doi.org/10.1126/science.1087576.

Amiel, E., Everts, B., Freitas, T.C., King, I.L., Curtis, J.D., Pearce, E.L., and Pearce, E.J. (2012). Inhibition of mechanistic target of rapamycin promotes dendritic cell activation and enhances therapeutic autologous vaccination in mice. J. Immunol. *189*, 2151–2158. https://doi.org/10.4049/jimmunol.1103741.

Amiel, E., Everts, B., Fritz, D., Beauchamp, S., Ge, B., Pearce, E.L., and Pearce, E.J. (2014). Mechanistic target of rapamycin inhibition extends cellular lifespan in dendritic cells by preserving mitochondrial function. J. Immunol. *193*, 2821–2830. https://doi.org/10.4049/jimmunol.1302498.

Artyomov, M.N., Munk, A., Gorvel, L., Korenfeld, D., Cella, M., Tung, T., and Klechevsky, E. (2015). Modular expression analysis reveals functional conservation between human Langerhans cells and mouse cross-priming dendritic cells. J. Exp. Med. *212*, 743–757. https://doi.org/10.1084/jem.20131675.

Bouteau, A., Kervevan, J., Su, Q., Zurawski, S.M., Contreras, V., Dereuddre-Bosquet, N., Le Grand, R., Zurawski, G., Cardinaud, S., Levy, Y., and Igyártó, B.Z. (2019). DC subsets regulate humoral immune responses by supporting the differentiation of distinct tfh cells. Front. Immunol. *10*, 1134. https://doi.org/10.3389/fimmu.2019.01134.

Brockstedt, D.G., Giedlin, M.A., Leong, M.L., Bahjat, K.S., Gao, Y., Luckett, W., Liu., W., Cook, D.N., Portnoy, D.A., and Dubensky, T.W., Jr. (2004). Listeria-based cancer vaccines that segregate immunogenicity from toxicity. Proc Natl Acad Sci USA *101*, 13832–7. https://doi.org/10.1073/pnas.0406035101.

Chávez-Arroyo, A., and Portnoy, D.A. (2020). Why is Listeria monocytogenes such a potent inducer of CD8+ T-cells? Cell Microbiol. *22*, e13175. https://doi.org/10.1111/cmi.13175.

Du, X., Wen, J., Wang, Y., Karmaus, P.W.F., Khatamian, A., Tan, H., Li, Y., Guy, C., Nguyen, T.L.M., Dhungana, Y., et al. (2018). Hippo/Mst signalling couples metabolic state and immune function of CD8α+ dendritic cells. Nature, 141–145. https://doi.org/10.1038/s41586-018-0177-0.

Edelson, B.T., Bradstreet, T.R., Hildner, K., Carrero, J.A., Frederick, K.E., Kc, W., Belizaire, R., Aoshi, T., Schreiber, R.D., Miller, M.J., et al. (2011). CD8α(+) dendritic cells are an obligate cellular entry point for productive infection by Listeria monocytogenes. Immunity *35*, 236–248. https://doi.org/10.1016/j.immuni.2011.06.012.

Eisenbarth, S.C. (2019). Dendritic cell subsets in T cell programming: location dictates function. Nat. Rev. Immunol. *19*, 89–103. https://doi.org/10.1038/s41577-018-0088-1.

Everts, B., Amiel, E., Huang, S.C.C., Smith, A.M., Chang, C.H., Lam, W.Y., Redmann, V., Freitas, T.C., Blagih, J., van der Windt, G.J.W., et al. (2014). TLR-driven early glycolytic reprogramming via the kinases TBK1-IKKε supports the anabolic demands of dendritic cell activation. Nat. Immunol. *15*, 323–332. https://doi.org/10.1038/ni.2833.

Everts, B., Amiel, E., van der Windt, G.J.W., Freitas, T.C., Chott, R., Yarasheski, K.E., Pearce, E.L., and Pearce, E.J. (2012). Commitment to glycolysis sustains survival of NO-producing inflammatory dendritic cells. Blood *120*, 1422–1431. https://doi.org/10.1182/blood-2012-03-419747.

Everts, B., Perona-Wright, G., Smits, H.H., Hokke, C.H., van der Ham, A.J., Fitzsimmons, C.M., Doenhoff, M.J., van der Bosch, J., Mohrs, K., Haas, H., Mohrs, M., Yazdanbakhsh, M., and Schramm, G. (2009). Omega-1, a glycoprotein secreted by Schistosoma mansoni eggs, drives Th2 responses. J Exp Med *206*, 1673–80. https://doi.org/10.1084/jem.20082460.

Fiegl, D., Kägebein, D., Liebler-Tenorio, E.M., Weisser, T., Sens, M., Gutjahr, M., and Knittler, M.R. (2013). Amphisomal route of MHC class I cross-presentation in bacteria-infected dendritic cells. J. Immunol. *190*, 2791–2806. https://doi.org/10.4049/jimmunol.1202741.

Foulds, K.E., Zenewicz, L.A., Shedlock, D.J., Jiang, J., Troy, A.E., and Shen, H. (2002). Cutting edge: CD4 and CD8 T cells are intrinsically different in their proliferative responses. J Immunol *168*, 1528–32. https://doi.org/10.4049/jimmunol.168.4.1528.

Fu, C., Liang, X., Cui, W., Ober-Blöbaum, J.L., Vazzana, J., Shrikant, P.A., Lee, K.P., Clausen, B.E., Mellman, I., and Jiang, A. (2015). β-Catenin in dendritic cells exerts opposite functions in cross-priming and maintenance of CD8 $^{+}$ T cells through regulation of IL-10. Proc. Natl. Acad. Sci. USA *112*, 2823–2828. https://doi.org/10.1073/pnas.1414167112.

Giladi, A., Cohen, M., Medaglia, C., Baran, Y., Li, B., Zada, M., Bost, P., Blecher-Gonen, R., Salame, T.M., Mayer, J.U., et al. (2020). Dissecting cellular crosstalk by sequencing physically interacting cells. Nat. Biotechnol. *38*, 629–637. https://doi.org/10.1038/s41587-020-0442-2.

Guak, H., Al Habyan, S., Ma, E.H., Aldossary, H., Al-Masri, M., Won, S.Y., Ying, T., Fixman, E.D., Jones, R.G., McCaffrey, L.M., and Krawczyk, C.M. (2018). Glycolytic metabolism is essential for CCR7 oligomerization and dendritic cell migration. Nat. Commun. *9*, 2463. https://doi.org/10.1038/s41467-018-04804-6.

Heieis, G.A., Patente, T.A., Tak, T., Almeida, L., and Everts, B. (2022). Spectral flow cytometry reveals metabolic heterogeneity in tissue macrophages. Preprint at bioRxiv. https://doi.org/10.1101/2022.05.26.493548.

Hildner, K., Edelson, B.T., Purtha, W.E., Diamond, M., Matsushita, H., Kohyama, M., Calderon, B., Schraml, B.U., Unanue, E.R., Diamond, M.S., et al. (2008). *Batf3* deficiency reveals a critical role for CD8α $^{+}$ dendritic cells in cytotoxic T cell immunity. Science *322*, 1097–1100. https://doi.org/10.1126/science.1164206.

Hilligan, K.L., Tang, S.C., Hyde, E.J., Roussel, E., Mayer, J.U., Yang, J., Wakelin, K.A., Schmidt, A.J., Connor, L.M., Sher, A., et al. (2020). Dermal IRF4+ dendritic cells and monocytes license CD4+ T helper cells to distinct cytokine profiles. Nat. Commun. *11*, 5637. https://doi.org/10.1038/s41467-020-19463-9.

Hussaarts, L., Smits, H.H., Schramm, G., van der Ham, A.J., van der Zon, G.C., Haas, H., Guigas, B., and Yazdanbakhsh, M. (2013). Rapamycin and omega-1: mTOR-dependent and-independent Th2 skewing by human dendritic cells. Immunol. Cell Biol. *91*, 486–489. https://doi.org/10.1038/icb.2013.31.

Igyártó, B., Haley, K., Ortner, D., Bobr, A., Gerami-Nejad, M., Edelson, B.T., Zurawski, S.M., Malissen, B., Zurawski, G., Berman, J., and Kaplan, D.H. (2011). Skin-resident murine dendritic cell subsets promote distinct and opposing antigen-specific T helper cell responses. Immunity *35*, 260–272. https://doi.org/10.1016/j.immuni.2011.06.005.

Jagannath, C., and Bakhru, P. (2012). Rapamycin-induced enhancement of vaccine efficacy in mice. Methods Mol. Biol. *821*, 295–303. https://doi.org/10.1007/978-1-61779-430-8_18.

Jagannath, C., Lindsey, D.R., Dhandayuthapani, S., Xu, Y., Hunter, R.L., Jr., and Eissa, N.T. (2009). Autophagy enhances the efficacy of BCG vaccine by increasing peptide presentation in mouse dendritic cells. Nat. Med. *15*, 267–276. https://doi.org/10.1038/nm.1928.

Janela, B., Patel, A.A., Lau, M.C., Goh, C.C., Msallam, R., Kong, W.T., Fehlings, M., Hubert, S., Lum, J., Simoni, Y., et al. (2019). A subset of type I conventional dendritic cells controls cutaneous bacterial infections through VEGFα-mediated recruitment of neutrophils. Immunity *50*, 1069–1083.e8. https://doi.org/10.1016/j.immuni.2019.03.001.

Jones, R.G., and Pearce, E.J. (2017). MenTORing immunity: mTOR signaling in the development and function of tissue-resident immune cells. Immunity *46*, 730–742. https://doi.org/10.1016/j.immuni.2017.04.028.

Kaplan, D.H. (2017). Ontogeny and function of murine epidermal Langerhans cells. Nat. Immunol. *18*, 1068–1075. https://doi.org/10.1038/ni.3815.

Kapsenberg, M.L. (2003). Dendritic-cell control of pathogen-driven T-cell polarization. Nat. Rev. Immunol. *3*, 984–993. https://doi.org/10.1038/nri1246.

Kellersch, B., and Brocker, T. (2013). Langerhans cell homeostasis in mice is dependent on mTORC1 but not mTORC2 function. Blood *121*, 298–307. https://doi.org/10.1182/blood-2012-06-439786.

Lawless, S.J., Kedia-Mehta, N., Walls, J.F., McGarrigle, R., Convery, O., Sinclair, L.V., Navarro, M.N., Murray, J., and Finlay, D.K. (2017). Glucose represses dendritic cell-induced T cell responses. Nat. Commun. *8*, 15620. https://doi.org/10.1038/ncomms15620.

Levin, C., Bonduelle, O., Nuttens, C., Primard, C., Verrier, B., Boissonnas, A., and Combadière, B. (2017). Critical role for skin-derived migratory DCs and Langerhans cells in T(FH) and GC responses after intradermal

immunization. J. Invest. Dermatol. *137*, 1905–1913. https://doi.org/10.1016/j.jid.2017.04.016.

Mach, N., Gillessen, S., Wilson, S.B., Sheehan, C., Mihm, M., and Dranoff, G. (2000). Differences in dendritic cells stimulated in vivo by tumors engineered to secrete granulocyte-macrophage colony-stimulating factor or Flt3-ligand. Cancer Res *60*. 3239–46.

Malinarich, F., Duan, K., Hamid, R.A., Bijin, A., Lin, W.X., Poidinger, M., Fairhurst, A.M., and Connolly, J.E. (2015). High mitochondrial respiration and glycolytic capacity represent a metabolic phenotype of human tolerogenic dendritic cells. J. Immunol. *194*, 5174–5186. https://doi.org/10.4049/jimmunol.1303316.

Marschall, P., Wei, R., Segaud, J., Yao, W., Hener, P., German, B.F., Meyer, P., Hugel, C., Ada Da Silva, G., Braun, R., et al. (2020). Dual function of Langerhans cells in skin TSLP-promoted T(FH) differentiation in mouse atopic dermatitis. J. Allergy Clin. Immunol., 1778–1794. https://doi.org/10.1016/j.jaci.2020.10.006.

Mashayekhi, M., Sandau, M.M., Dunay, I.R., Frickel, E.M., Khan, A., Goldszmid, R.S., Sher, A., Ploegh, H.L., Murphy, T.L., Sibley, L.D., and Murphy, K.M. (2011). CD8α(+) dendritic cells are the critical source of interleukin-12 that controls acute infection by Toxoplasma gondii tachyzoites. Immunity *35*, 249–259. https://doi.org/10.1016/j.immuni.2011.08.008.

Maynard, S.K., Marshall, J.D., MacGill, R.S., Yu, L., Cann, J.A., Cheng, L.I., McCarthy, M.P., Cayatte, C., and Robbins, S.H. (2019). Vaccination with synthetic long peptide formulated with CpG in an oil-in-water emulsion induces robust E7-specific CD8 T cell responses and TC-1 tumor eradication. BMC Cancer *19*, 540. https://doi.org/10.1186/s12885-019-5725-y.

Mintern, J.D., Macri, C., Chin, W.J., Panozza, S.E., Segura, E., Patterson, N.L., Zeller, P., Bourges, D., Bedoui, S., McMillan, P.J., et al. (2015). Differential use of autophagy by primary dendritic cells specialized in cross-presentation. Autophagy *11*, 906–917. https://doi.org/10.1080/15548627.2015.1045178.

Ohtani, M., Hoshii, T., Fujii, H., Koyasu, S., Hirao, A., and Matsuda, S. (2012). Cutting edge: mTORC1 in intestinal CD11c+ CD11b+ dendritic cells regulates intestinal homeostasis by promoting IL-10 production. J. Immunol. *188*, 4736–4740. https://doi.org/10.4049/jimmunol.1200069.

Patente, T.A., Pelgrom, L.R., and Everts, B. (2019). Dendritic cells are what they eat: how their metabolism shapes T helper cell polarization. Curr. Opin. Immunol. *58*, 16–23. https://doi.org/10.1016/j.coi.2019.02.003.

Pelgrom, L.R., Patente, T.A., Sergushichev, A., Esaulova, E., Otto, F., Ozir-Fazalalikhan, A., van der Zande, H.J.P., van der Ham, A.J., van der Stel, S., Artyomov, M.N., and Everts, B. (2019). LKB1 expressed in dendritic cells governs the development and expansion of thymus-derived regulatory T cells. Cell Res. *29*, 406–419. https://doi.org/10.1038/s41422-019-0161-8.

Qiu, C.C., Atencio, A.E., and Gallucci, S. (2019). Inhibition of fatty acid metabolism by etomoxir or TOFA suppresses murine dendritic cell activation without affecting viability. Immunopharmacol. Immunotoxicol. *41*, 361–369. https://doi.org/10.1080/08923973.2019.1616754.

Reinicke, A.T., Omilusik, K.D., Basha, G., and Jefferies, W.A. (2009). Dendritic cell cross-priming is essential for immune responses to Listeria monocytogenes. PLoS One *4*, e7210. https://doi.org/10.1371/journal.pone.0007210.

Riebisch, A.K., Mühlen, S., Beer, Y.Y., and Schmitz, I. (2021). Autophagy-a story of bacteria interfering with the host cell degradation machinery. Pathogens *10*, 110. https://doi.org/10.3390/pathogens10020110.

Saxton, R.A., and Sabatini, D.M. (2017). mTOR signaling in growth, metabolism, and disease. Cell *168*, 960–976. https://doi.org/10.1016/j.cell.2017.02.004.

Seneschal, J., Jiang, X., and Kupper, T.S. (2014). Langerin+ dermal DC, but not Langerhans cells, are required for effective CD8-mediated immune responses after skin scarification with vaccinia virus. J. Invest. Dermatol. *134*, 686–694. https://doi.org/10.1038/jid.2013.418.

Sinclair, C., Bommakanti, G., Gardinassi, L., Loebbermann, J., Johnson, M.J., Hakimpour, P., Hagan, T., Benitez, L., Todor, A., Machiah, D., et al. (2017). mTOR regulates metabolic adaptation of APCs in the lung and controls the outcome of allergic inflammation. Science, 1014–1021. https://doi.org/10.1126/science.aaj2155.

Snyder, J.P., and Amiel, E. (2018). Regulation of dendritic cell immune function and metabolism by cellular nutrient sensor mammalian target of rapamycin (mTOR). Front. Immunol. *9*, 3145. https://doi.org/10.3389/fimmu.2018.03145.

Sun, Y., Oravecz-Wilson, K., Bridges, S., McEachin, R., Wu, J., Kim, S.H., Taylor, A., Zajac, C., Fujiwara, H., Peltier, D.C., et al. (2019). miR-142 controls metabolic reprogramming that regulates dendritic cell activation. J. Clin. Invest. *129*, 2029–2042. https://doi.org/10.1172/JCI123839.

Theisen, D.J., Davidson, J.T.t., Briseno, C.G., Gargaro, M., Lauron, E.J., Wang, Q., Desai, P., Durai, V., Bagadia, P., et al. (2018). WDFY4 is required for cross-presentation in response to viral and tumor antigens. Science *362*, 694–699. https://doi.org/10.1126/science.aat5030.

Thwe, P.M., and Amiel, E. (2018). The role of nitric oxide in metabolic regulation of Dendritic cell immune function. Cancer Lett. *412*, 236–242. https://doi.org/10.1016/j.canlet.2017.10.032.

Thwe, P.M., Pelgrom, L.R., Cooper, R., Beauchamp, S., Reisz, J.A., D'Alessandro, A., Everts, B., and Amiel, E. (2017). Cell-intrinsic glycogen metabolism supports early glycolytic reprogramming required for dendritic cell immune responses. Cell Metabol. *26*, 558–567.e5. https://doi.org/10.1016/j.cmet.2017.08.012.

van Panhuys, N., Klauschen, F., and Germain, R.N. (2014). T-cell-receptor-dependent signal intensity dominantly controls CD4(+) T cell polarization *in vivo*. Immunity *41*, 63–74. https://doi.org/10.1016/j.immuni.2014.06.003.

Villanueva, M.S., Sijts, A.J., and Pamer, E.G. (1995). Listeriolysin is processed efficiently into an MHC class I-associated epitope in Listeria monocytogenes-infected cells. J. Immunol. *155*, 5227–5233.

Weichhart, T., Hengstschläger, M., and Linke, M. (2015). Regulation of innate immune cell function by mTOR. Nat. Rev. Immunol. *15*, 599–614. https://doi.org/10.1038/nri3901.

Wu, D., Sanin, D.E., Everts, B., Chen, Q., Qiu, J., Buck, M.D., Patterson, A., Smith, A.M., Chang, C.H., Liu, Z., et al. (2016). Type 1 interferons induce changes in core metabolism that are critical for immune function. Immunity *44*, 1325–1336. https://doi.org/10.1016/j.immuni.2016.06.006.

Yao, C., Zurawski, S.M., Jarrett, E.S., Chicoine, B., Crabtree, J., Peterson, E.J., Zurawski, G., Kaplan, D.H., and Igyártó, B.Z. (2015). Skin dendritic cells induce follicular helper T cells and protective humoral immune responses. J. Allergy Clin. Immunol. *136*, 1387–1397.e7. https://doi.org/10.1016/j.jaci.2015.04.001.

Zimara, N., Florian, C., Schmid, M., Malissen, B., Kissenpfennig, A., Männel, D.N., Edinger, M., Hutchinson, J.A., Hoffmann, P., and Ritter, U. (2014). Langerhans cells promote early germinal center formation in response to Leishmania-derived cutaneous antigens. Eur. J. Immunol. *44*, 2955–2967. https://doi.org/10.1002/eji.201344263.

STAR★METHODS

KEY RESOURCES TABLE

REAGENT or RESOURCE	SOURCE	IDENTIFIER
Antibodies		
CD11b (Clone: M1/70; PE-Cy7)	Invitrogen/eBioscience	Cat# 25-0112-82; RRID: AB_469588
CD11b (Clone: M1/70; BUV563)	BD Biosciences	Cat# 565976; RRID: AB_2738276
CD11c (Clone: N418; BV421)	BioLegend	Cat# 117330; RRID: AB_1121959
CD11c (Clone: N418; PE-Cy7)	Invitrogen/eBioscience	Cat# 25-0114-82; RRID: AB_469590
CD11c (Clone: N418; BUV496)	BD Biosciences	Cat# 750450; RRID: AB_2874611
CD19 (Clone: eBio1D3; ef450)	Invitrogen/eBioscience	Cat# 48-0193-82; RRID: AB_2734905
CD172a (Clone: P84; Biotin)	BioLegend	Cat# 144026; RRID: AB_2721320
CD172a (Clone: P84; PE)	BioLegend	Cat# 144011; RRID: AB_2563549
CD172a (Clone: P84; BUV805)	BD Biosciences	Cat# 741997; RRID: AB_2871296
CD197 (CCR7) (Clone: 4B12; BV605)	BioLegend	Cat# 120125; RRID: AB_2715777
CD25 (Clone: PC61; PerCP-Cy5.5)	BD Biosciences	Cat# 551071; RRID: AB_394031
CD24 (Clone: M1/69; APC/Fire 750)	BioLegend	Cat# 101839; RRID: AB_2650875
CD274 (PD-L1) (Clone: MIH5; BUV737)	BD Biosciences	Cat# 741877; RRID: AB_2871203
CD3 (Clone: 17A2; FITC)	Invitrogen/eBioscience	Cat# 11-0032-82; RRID: AB_2572431
CD3 (Clone: 17A2; eF450)	Invitrogen/eBioscience	Cat# 48-0032-82; RRID: AB_1272193
CD3 (Clone: 17A2; BV605)	BioLegend	Cat# 100237; RRID: AB_2562039
CD3 (Clone: 17A2; APC)	Invitrogen/eBioscience	Cat# 17-0032-82; RRID: AB_10597589
CD3 (Clone: 17A2; BV750)	Biolegend	Cat# 100249; RRID: AB_2734148
CD3 (Clone: 17A2; PercP F710)	Invitrogen/eBioscience	Cat# 46-0032-82; RRID: AB_1834427
CD36 (Clone: HM36; AF 700)	Invitrogen/eBioscience	Cat# 56-0362-82; RRID: AB_2811887
CD326 (Clone: G8.8; BV605)	BioLegend	Cat# 118227; RRID: AB_2563984
CD326 (Clone: G8.8; APC/Fire 750)	BioLegend	Cat# 118229; RRID: AB_2629757
CD326 (Clone: G8.8; AF594)	Biolegend	Cat# 118222; RRID: AB_2563322
CD4 (Clone: GK1.5; PE-Cy7)	Invitrogen/eBioscience	Cat# 25-0041-81; RRID: AB_469576
CD4 (Clone: GK1.5; PerCP-eF710)	Invitrogen/eBioscience	Cat# 46-0041-82; RRID: AB_11150050
CD4 (Clone: GK1.5; BV650)	BD Biosciences	Cat# 563232; RRID: AB_2738083
CD40 (Clone: HM40-3; FITC)	Invitrogen/eBioscience	Cat# 11-0402-82; RRID: AB_465029
CD44 (Clone: IM7; eF450)	Invitrogen/eBioscience	Cat# 48-0441-82; RRID: AB_1272246
CD44 (Clone: IM7; PE-Cy7)	Invitrogen/eBioscience	Cat# 25-0441-81; RRID: AB_469623
CD45 (Clone: 30-F11; APC Fire810)	Biolegend	Cat# 103173; RRID: AB_2860599
CD62L (Clone: MEL-14; APC-eF780)	Invitrogen/eBioscience	Cat# 47-0621-82; RRID: AB_1603256
CD64 (Clone: X54-5/7.1; BV711)	Biolegend	Cat# 139311; RRID: AB_2563846
CD70 (Clone: FR70; biotin)	BioLegend	Cat# 104603; RRID: AB_313116
CD8a (Clone: 53-6.7; BV711)	BioLegend	Cat# 100747; RRID: AB_11219594
CD80 (Clone: 16-10A1; PE)	Invitrogen/eBioscience	Cat# 553769; RRID: AB_395039
CD86 (Clone: GL-1; PerCp-Cy5.5)	BioLegend	Cat# 105028; RRID: AB_2074994
CD86 (Clone: GL-1; BV510)	Biolegend	Cat# 105039; RRID: AB_2562370
CD98 (Clone: H202-141; BUV615)	BD Biosciences	Cat# 752360; RRID: AB_2875877
CD8a (Clone: 53-6.7; APC)	Tonbo Biosciences	Cat# 20-0081-U025
CD8a (Clone: 53-6.7; APC-Cy7)	BioLegend	Cat# 100714; RRID: AB_312753
CD8a (Clone: 53-6.7; PE)	Invitrogen/eBioscience	Cat# 12-0081-83; RRID: AB_465530
B220 (Clone: RA3-6B2; ef450)	Invitrogen/eBioscience	Cat# 48-0452-82; RRID: AB_1548761
B220 (Clone: RA3-6B2; Pe-Cy5)	BD Bioscience	Cat# 553091; RRID: AB_394621

(*Continued on next page*)

Continued

REAGENT or RESOURCE	SOURCE	IDENTIFIER
Goat anti-rabbit (Clone: -; AF647)	Invitrogen	Cat# A27040; RRID: AB_2536101
HPV tetramer (Clone: -; APC)	in house	Cat# -
Ly6C (Clone: HK1.4; PerCP-Cy5.5)	Invitrogen/eBioscience	Cat# 45-5932-80; RRID: AB_2723342
Ly6G (Clone: 1A8; SB550)	BioLegend	Cat# 108467; RRID: AB_2876421
IFNγ (Clone: XMG1.2; PE-Cy7)	Invitrogen/eBioscience	Cat# 25-7311-82; RRID: AB_469680
IFNγ (Clone: XMG1.2; APC-Cy7)	BD Biosciences	Cat# 561479; RRID: AB_10898181
IFNγ (Clone: XMG1.2; FITC)	Invitrogen/eBioscience	Cat# 11-7311-41; RRID: AB_10718840
IL-10 (Clone: JES5-16E3; AF488)	Invitrogen/eBioscience	Cat# 53-7101-82; RRID: AB_469926
IL-12p40/p70 (Clone: C15.6; APC)	BD Biosciences	Cat# 554480; RRID: AB_398560
IL-17A (Clone: eBio17B7; APC)	Invitrogen/eBioscience	Cat# 17-7177-81; RRID: AB_763580
IL-4 (Clone: BVD4-1D11; PE)	BD Biosciences	Cat# 554389; RRID: AB_395361
Kb-SIINFEKL (Clone: 25-D1-16; PE)	BioLegend	Cat# 141604; RRID: AB_10895905
MHC II (Clone: M5/114.15; FITC)	Invitrogen/eBioscience	Cat# 11-5321-82; RRID: AB_465232
MHCI (Clone: AF6-88.5; AF647)	BioLegend	Cat# 116511; RRID: AB_492918
MHCII (Clone: M5/114.15.2; AF700)	Invitrogen/eBioscience	Cat# 56-5321-80; RRID: AB_494010
MHC II (Clone: 2G9; BUV 395)	BD Bioscience	Cat# 743876; RRID: AB_2741827
MHCII (Clone: M5/114.15.2; APC-eF780)	Invitrogen/eBioscience	Cat# 47-5321-82; RRID: AB_1548783
OVA tetramer (Clone: -, PE)	in house	-
pS6 (ser240) (Clone: N4-41; PE)	Invitrogen/eBioscience	Cat# 560430; RRID: AB_2572667
Siglec-H (Clone: 511; APC)	BioLegend	Cat# 129611; RRID: AB_10643574
Siglec-F (Clone: E50-2440; BV480)	BD Biosciences	Cat# 746668; RRID: AB_2743940
Streptavidin (Clone: -; PerCP-Cy5.5)	BioLegend	Cat# 405214
Streptavidin (Clone: -; BV605)	BioLegend	Cat# 405229
Streptavidin (Clone: -; BV785)	BioLegend	Cat# 405249
XCR1 (Clone: ZET; BV650)	BioLegend	Cat# 148220; RRID: AB_2566410
XCR1 (Clone: ZET; BV421)	BioLegend	Cat# 148216; RRID: AB_2565230
Glut1 (Clone: EPR3915; Dylight 405)	AbCam	Cat# ab252403
PKM (Clone: EPR10138(B); PE)	AbCam	Cat# ab206129
Cytc (Clone: 7H8.2C12; PE-Cy7)	AbCam	Cat# ab237966
G6PD (Clone: EPR20668; APC-Cy7)	AbCam	Cat# ab231828
CPT1A (Clone: EPR21843-71-2F; PE-Cy5)	AbCam	Cat# ab235841
ACC1 (Clone: EPR23235-147; AF488)	AbCam	Cat# ab272704
SDHA (Clone: EPR9043(B); AF647)	AbCam	Cat# ab240098
Bacterial and virus strains		
OVA-expressing *Listeria monocytogenes*	Gift from S Schoenberger (La Jolla, USA)	Foulds et al., 2002
OVA-expressing *Listeria monocytogenes* strain deficient in actin assembly-inducing protein (Lm-dActA-OVA)	Gift from S Schoenberger (La Jolla, USA)	Brockstedt et al., 2004
Chemicals, peptides, and recombinant proteins		
CellTraceTM Violet Cell proliferation Kit	Invitrogen™	Cat# C34557
LIVE/DEAD Fixable Aqua Dead Cell Stain Kit	Thermo Fischer Scientific	Cat#L34965
LIVE/DEAD Fixable Blue Dead Cell Stain Kit	Thermo Fischer Scientific	Cat# L34962
OVA SIINFEKL peptide	In house	N/A
Ovalbumin	InvivoGen	Cat# vac-pova-100
PolyIC	InvivoGen	Cat# TLRL-PIC
CpG-B	InvivoGen	Cat# TLRL-1826-1
LPS	InvivoGen	Cat# TLRL-PELPS
MitoTracker Green	Invitrogen	Cat# M7514

(*Continued on next page*)

Continued

REAGENT or RESOURCE	SOURCE	IDENTIFIER
MitoTracker DeepRed	Invitrogen	Cat# M22426
TMRM	Thermo	Cat# T668
2-NBDG	Invitrogen	Cat# N13195
Phorbol 12-myristate 13-acetate (PMA)	Sigma	Ca# P-8139t
Ionomycin	Sigma	Cat# I-0634
Brefeldin A	Sigma	Cat# B7651
RPMI 1640 GlutaMAX	Gibco	Cat# 61870-010
Colagenase D	Roche	Cat# 11088866001
DNAse I	Sigma	Cat# D4263
FITC	Sigma	Cat# F3651
Dibutylphalate	Sigma	Cat# 524980
Critical commercial assays		
Foxp3/transcription factor staining buffer set	eBioscience	Cat# 00-5523-00
Bicinchoninic acid (BCA) protein assay kit	Pierce	Cat# PIER23225
Experimental models: Cell lines		
Flt3L-secreting B16 melanoma cells	Gift from E Pearce (Washington University, USA)	Mach et al., 2000
Experimental models: Organisms/strains		
Mouse: C57BL/6J	The Jackson Laboratory	JAX:000664
Mouse: Itgax-cre	The Jackson Laboratory	JAX:008068
Mouse: Rptor-fl/fl	The Jackson Laboratory	JAX:013188
Mouse: OT II BL/6J	The Jackson Laboratory	JAX:004194
Mouse: OT I BL/6J	The Jackson Laboratory	JAX:003831
Software and algorithms		
FlowJo v10	TreeStar	www.flowjo.com
GraphPad Prism v9	GraphPad Software	www.graphpad.com
OMIQ	OMIQ	www.omiq.ai

RESOURCE AVAILABILITY

Lead contact

Further information and requests for resources and reagents should be directed to and will be fulfilled by the lead contact, Bart Everts (b.everts@lumc.nl).

Materials availability

This study did not generate new unique reagents.

Data and code availability

All data reported in this paper will be shared by the lead contact upon request. This paper does not report original code. Any additional information required to reanalyze the data reported in this paper is available from the lead contact upon request.

EXPERIMENTAL MODEL AND SUBJECT DETAILS

Mice

Itgax-cre Rptor-fl/fl (CD11c-cre raptor-fl/fl or CD11c$^{\Delta raptor}$ mice), transgenic with OVA specific CD4 T cells (OT-II), transgenic with OVA specific CD8+ T cells (OT-I) and wild type (WT) mice, both male and female and all on a C57BL/6J background, were bred under SPF conditions at the Leiden University Medical Center (LUMC), Leiden, The Netherlands. Mice were culled through cervical dislocation. Anaesthesia with isoflurane was used for *L. monocytogenes infection* and ketamine with either dexdomitor or xylazine was used for *S. mansoni* infection. Animal experiments were performed when the mice were between 8 and 16 weeks old. Animal experiments were performed in accordance with local government regulations, EU Directive 2010/63EU and Recommendation

2007/526/EC regarding the protection of animals used for experimental and other scientific purposes, as well as approved by the Dutch Central Authority for Scientific Procedures on Animals (CCD). Animal license number AVD116002015253.

Flt3L-secreting B16 melanoma cells

Flt3L-secreting B16 melanoma cells were kindly provided by Dr. Edward Pearce and passaged every 3–4 days using a Trypsin-EDTA solution (Sigma, Zwijndrecht, The Netherlands) followed by replating in T175 culture flasks at 2 × 10^6 cells in 35 mL of media comprised of DMEM High Glucose (Biowest, Nuaillé, France) supplemented with 10% FCS (Capricorn, Den Haag, The Netherlands), 100 U/mL penicillin (Eureco-pharma, Ridderkerk, The Netherlands) and 100 μg/mL streptomycin (Sigma).

METHOD DETAILS

Digestion of murine tissues

Lymphoid organs were collected in 500 μL of no additives media (naRPMI = RPMI-1640 supplemented with GlutaMAX™ [#61870-010, Gibco, Bleiswijk, The Netherlands], which should contain Ca^{2+} for the collagenase) in a plate and mechanically disrupted using the back-end of a syringe before addition of 50 μL of a digestion media (dRPMI = naRPMI supplemented with 11× collagenase D (#11088866001, Roche, Woerden, The Netherlands; end concentration of 1 mg/mL) and 11× DNase I (#D4263, Sigma, Zwijndrecht, The Netherlands; end concentration of 2000 U/mL) for 20 min at 37°C and 5% CO_2. Single cell suspensions were filtered after digestion with a 100 μm sterile filter (#352360, BD Biosciences, Vianen, The Netherlands) before counting in complete RMPI (cRPMI = naRPMI supplemented with 10% heat-inactivated FCS [#S-FBS-EU-015, Serana, Pessin, Germany], 25 nM β-mercaptoethanol [#M6250, Sigma], 100 U/mL penicillin [#16128286, Eureco-pharma, Ridderkerk, The Netherlands; purchased inside the LUMC] and 100 μg/mL streptomycin [#S9137, Sigma]). Spleens were subjected to red blood cell lysis (inhouse; 0.15 M NH4Cl, 1 mM KHCO3, 0.1 mM EDTA [#15575-038, Thermo, Waltham, Massachusetts, United States] in ddH20) for 2 min at room temperature before counting.

Generation of bone marrow-derived GMDCs

BM cells were flushed from mouse femurs and tibia and plated in 'Nunc™ Cell-Culture Treated 6-well plate' wells (#140675, Thermo; approximate growth area of 9.5 cm^2) at a seeding density of 2 × 10^6 cells in a volume of 3 mL of complete RPMI for BM cells (cRPMI-BM = RPMI-1640 supplemented with GlutaMAX™ and also 5% FCS, 25 nM β-mercaptoethanol, 100 U/mL penicillin and 100 μg/mL streptomycin was put in) to which 20 ng/mL of recombinant GM-CSF (#315-03, PeproTech, Hamburg, Germany) was added. Media was refreshed on day 3–4 by adding 3 mL cRPMI-BM with 40 ng/mL GM-CSF and on day 7 by first removing 3 mL of supernatant and then adding 3 mL cRPMI-BM with 40 ng/mL GM-CSF. Semi-adherent cells were harvested for various assays on day 8. Alternatively, semi-adherent cells were collected on day 7 and seeded in a flat bottom 96-well plate (Nunc™; #167008, Thermo) at 1 × 10^5 cells in a volume of 200 μL of fresh cRPMI-BM with 20 ng/mL GM-CSF and rested overnight. Minimum rest time after transfer of GMDCs was 2–3 h.

Flow cytometry

In general, single cell suspensions underwent viability staining for 20 min at room temperature using the LIVE/DEAD™ Fixable Aqua (#L34957, Thermo; 1:400 in PBS [from LUMC pharmacy; Braun, Zeist, The Netherlands) or Blue (#L23105, Thermo; 1:1000 in PBS) and fixation for 15 min at room temperature using 1.85% formaldehyde (F1635, Sigma) in PBS solution before surface staining with antibodies in an in-house cell separation buffer (= PBS supplemented with 0.5% BSA [fraction V, #10735086001, Roche, Woerden, The Netherlands] and 2 mM EDTA) for 30 min at 4°C. For detection of metabolic proteins cells were permeabilized with eBioscience permeabilization buffer (#00-8333-56 – Thermo) followed by intracellular staining with a cocktail of antibodies against the metabolic proteins. Antibodies were purchased from AbCam and conjugated in house with AbCam Lightening-Link Conjugation kit. See supplementary Table S1 for further information on metabolic antibodies and fluorochrome conjugation. For detection of phosphorylated S6 on Ser235/236, single cell suspensions in cRPMI where returned to a cell incubator (37°C & 5% CO_2) for 1 h after which 16% μLtra-pure formaldehyde (#18814-20, Polysciences, Hirschberg an der Bergstraβe, Germany) was added until the concentration reached 4% and the cells were left for 10 more minutes in the incubator to fix. For example, 67 μL of 16% μLtra-pure formaldehyde was added to 200 μL of cell solution. Viability staining was not done before fixation to minimise changes in phosphorylation status. Single cell suspensions were first stained with anti-phosphorylated S6 in 1× Permeabilization Buffer (#00-8333-56, Thermo) for 1 h at room before staining with other antibodies in the in-house cell separation buffer for 30 min at 4°C. For detection of mitochondrial mass and mitochondrial membrane potential, single cell suspensions were incubated with respectively 200 nM MitoTracker Green (#M7514, Invitrogen) or 200 nM TMRM (#T668, Thermo) in cRPMI for 30 min in a cell incubator. Subsequent viability and surface staining were done for 30 min on ice. No fixation occurred before running the samples. Uptake of 2-NBDG (N13195, Invitrogen) was done in a similar fashion but with 15 min of incubation. CD8+ T cells bearing antigen-specific T cell receptors were quantified using in-house produced tetramers of MHCI:peptide complexes with SIINFEKL (K^bOVA-tetramer) or RAHYNIVTF (D^bE7-tetramer) as their respective epitopes. For detection of antigen-specific cytokine production by T cells, single cell suspensions in cRPMI were restimulated with either 1 μg/mL of SIINFEKL (in-house) or 1 μg/mL of RAHYNIVTF (in-house) in the presence of 10 μg/mL of Brefeldin A (#B7651, Sigma) for 4 h in a cell incubator. For polyclonal restimulation, single cell suspensions were stimulated

with both 0.1 μg/mL of PMA (#P-8139, Sigma) and 1 μg/mL of ionomycin (#I-0634, Sigma) in the presence of Brefeldin A. These single cell suspensions underwent intracellular cytokine staining (ICS) with antibodies in the 1× Permeabilization Buffer. For detection of IL-12 by DCs, single cell suspensions were stimulated with either 100 ng/mL of LPS, 10 μg/mL of PolyIC or 5 μg/mL of CpG-B (#TLRL-PELPS, #TLRL-PIC and #tlrl-1826-1, respectively [all InvivoGen, Toulouse, France]) and all in the presence of Brefeldin A for 5 h in a cell incubator. Cross presentation was quantified by surface staining with an anti-Kb-SIINFEKL antibody after 3 h of stimulation with OVA SLP (in house; 50 μg/mL for skin draining lymph node cells) in the presence of 10 μg/mL PolyIC. SIINFEKL (1 μg/mL) was used as positive MHCI loading control. All samples were run on a BD LSR II,FACSCanto II or Cytek Aurora 5 lasers and analyzed using FACS Diva 8 (all BD Biosciences) and FlowJo (Version 10, TreeStar, Meerhout, Belgium).

High dimensional spectral flow cytometry analysis

Samples were imported in OMIQ software and parameters were scaled using a conversion factors ranging from 6000-20000. Samples were subsequently gated on DCs and subsampled using a maximum equal distribution across groups. After sub-sampling, opt-SNE was performed using the metabolic proteins and lineage markers (CD172a, XCR1 and CD326) as parameters. Next, phenograph clustering (k = 100) was performed using the same parameters used for the opt-SNE. Data was further analysed with EdgeR to determine significant differences in the clusters among different genotypes. Heatmaps and volcano plots were generated in R, using OMIQ-exported data for each cluster.

In vitro co-culture of DCs and OT I T cells

Mice were subcutaneously injected with either PBS or 25 μg of CpG-B with 50 ug of OVA for 24 h. LCs from IngLNs were purified by FACS and 4 mice per genotype were pooled. LCs were then incubated with CTV pre-labelled OT-I T cells in a ratio of 1:50 (1000 LC:50000 T cells) either in the presence or absence of OT-I peptide (1 μg/mL). After 3 days, T cells were harvested and the dilution of CTV was evaluated as a proxy for proliferation. *In vitro* cross-presentation assays was performed using 10000 sorted splenic cDC1s and 25000 CTV-labelled OT-I cells in the presence of 10 million HKLM-OVA, as previously described (Theisen et al., 2018). After 3 days OT-I cells were harvested and CTV proliferation was evaluated by flow cytometry.

In vivo DC-T cell interaction

Mice were subcutaneously injected with either PBS or 25 μg of CpG-B with 50 ug of OVA for 24 h. IngLn was collected, digested with a mild digestion mix (1 mg/mL of collagenase D for 30 min at 37°C) to preserve the interaction between cells. Cell suspension was then stained with anti-CD3, anti-CD19, anti-CD8, anti-MHC II, anti-Siglec-H, anti-XCR1 and anti-CD326. Analysis was performed as previously described (Giladi et al., 2020). Briefly, after exclusion of B cells and pDCs, frequency of doublets expressing $CD3^+CD8^+$ as well as $MHCII^+$ and DC subset-specific markers were quantified by flow cytometry.

Preparation of *Listeria monocytogenes* bacteria

Listeria monocytogenes bacteria were scraped from a glycerol stock and transferred to a 15 mL round bottom polysterene tube (#352051, Corning, Amsterdam, The Netherlands) with 3 mL of 'Brain Heart Infusion (BHI) Broth' (#37500, BD Biosciences) and incubated overnight at 37° with the cap loose and the tube rotating at 200 rpm. The next day, 20 and 50 μL of bacteria solution was transferred to new tubes with broth and cultured for another 3 h. The optical density (OD) was measured at 600 nm (OD600) using a spectrophotometer (#Ultrospec 100 pro, GE Healthcare, Hoevelaken, The Netherlands after takeover of Amersham Biosciences by GE Healthcare) and the concentration of bacteria solution was corrected until the OD600 value corresponded approximately to 1.2 × 10^8 colony forming units (CFU) per mL of broth, which was previously determined by titration. To make new glycerol stocks, 1 mL of the overnight cultured bacterial solution and 500 μL of pure glycerol were mixed well and stored at −80°.

Listeria *monocytogenes* infection and challenge

Mice were infected with a live attenuated OVA-expressing *L. monocytogenes* strain deficient in actin assembly-inducing protein (Lm-dActA-OVA), which is required for escape from phagosomes and cell-to-cell spreading (Poussin, Cell Res 2010). Bacteria were centrifuged at 2000 rpm for 10 min at 4° and brought to 2.5×10^7 CFU per mL of PBS. Mice were sedated with isoflurane and infected by retro-orbital intravenous (i.v.) injection with 200 μL of bacteria in PBS (=5×10^6 CFU). The remaining bacteria were brought to 10^3 CFU per mL of PBS and 50 μL of this bacteria solution (=50 CFU) was plated on a 'BHI Agar Plate' (#255003, BD Biosciences) and incubated overnight at 37° for control counting of colonies next day. Mice were culled 7 days later, and organs were processed as described above. Alternatively, 21 days after infection, mice were challenged with 5×10^4 OVA-expressing wild type bacteria (Lm-OVA) in 200 μL of PBS by retro-orbital i.v. injection and at day 24, mice were culled, and organs were processed as described above. Bacterial load in the organs was determined by taking 100 μL of a 5 mL single cell suspension in PBS and lysing this in 900 μL 0.1% Triton X-100 (T8532, Sigma) in mQ (1:10 single cell suspension:0.1% Triton) and making further dilutions of 1:100 and 1:1000 before plating on a agar plate and overnight incubation at 37° for control counting of colonies the next day.

In vivo cDC expansion, isolation, sorting and transfer

The *in vivo* expansion of cDCs using Flt3L-secreting B16 melanoma cells and their subsequent sorting, *ex vivo* conditioning and transfer into recipient mice to induce DC-specific T cell responses was done as described previously (Pelgrom et al., 2019).

cDC1s were stimulated with 100 μg/mL of ovalbumin (OVA; #vac-pova-100, InvivoGen) and 10 μg/mL of PolyIC. 300.000 cells were transferred.

Preparation of Schistosoma mansoni soluble egg antigens

S. mansoni eggs were isolated and processed into a SEA preparation as described previously (Everts et al., 2009). Protein concentration was determined using a bicinchoninic acid (BCA) protein assay kit (Pierce, #PIER23225). Endotoxin contamination was determined by a direct comparison of SEA batches to LPS in a TLR4-transfected Human Embryonic Kidney 293 (HEK) reporter cell line, in which IL-8 secretion by 5×10^8 HEK cells after stimulation with 10 μg of SEA is expected to be similar or less than after stimulation with 1–3 ng/mL of LPS.

Schistosoma mansoni acute infection

Mice were infected with *S. mansoni* (Puerto Rican strain; Naval Medical Research Institute) by 30 min of percutaneous exposure to 60 cercariae (or up to 100 cercariae) on shaved abdomen. Mice were culled 8 weeks later. Cercariae were kept at 30 cercariae per mL of store bought Barleduc water, which was kept very carefully at 31°C. Female mice were anesthetized by intraperitoneal (i.p) injection with 300 μL of 50 mg/kg bodyweight ketamine +0.5 mg/kg bodyweight dexdomitor, while male mice were anesthetized with 50 mg/kg bodyweight ketamine +10 mg/kg bodyweight xylazine. Female mice were assisted in waking up by i.p. injection with 150 μL of 0.4 mg/kg bodyweight antisedan. All injections were done using PBS and a 25G needle. All anaesthetics were bought at the LUMC pharmacy. Livers were processed like spleens except that single cell suspensions were centrifuged twice at 20 g for 10 min in PBS to remove hepatocytes before red blood cell lysis.

In vivo T cell priming and DC activation following immunization

For evaluation of T cell priming, mice were injected s.c. either with a) 5 μg of LPS together with 25 μg of OVA and emulsified in 40 μL of incomplete Freunds' adjuvant (IFA; #vac-ifa-10, InvivoGen) in the hind footpad, or b) 10–25 μg of CpG-B with OVA and in IFA in the footpad, or c) 25 μg of PolyIC with 100 μg of E7-SLP in 50 μL of PBS in the tailbase, or d) 25 μg of CpG-B with E7-SLP in PBS in the tailbase. Mice were culled 7 days later and draining popLNs were collected after footpad injection and draining ingLNs were collected after tailbase injection. For evaluation of DC activation, OVA- and E7-SLP were omitted and draining LNs were collected after 24 h instead of 7 days.

Cytometric bead array

Cell culture supernatants were analysed for IFNγ, IL-4, IL-5, IL-10 and IL-13 secretion using a cytokine bead array (#I558296, #558298, #558302, #558300 and #558349 respectively and all BD Biosciences) on a flow cytometer as recommended by the manufacturer, but with both the beads and antibodies diluted 1:10 relative to the original recommendation.

FITC painting

Mice were painted with 20 μL of inflammatory FITC paint (5 mg/mL fluorescein isothiocyanate [#F3651, Sigma] in a 1:1 mix of dibutylphalate [#524980, Sigma] and acetone [#100014, Merck, Amsterdam, The Netherlands]) on shaved flanks and draining ingLNs were collected either 1 or 3 days later.

QUANTIFICATION AND STATISTICAL ANALYSIS

Statistical analysis as specified in figure legends were performed with Prism 9 (GraphPad software Inc., San Diego, California, United States). When differences between two groups were analysed, unpaired Student's t test was used; when differences between more than two groups were analysed, the one-way unpaired analysis of variance (ANOVA) corrected for multiple comparisons using Tukey's multiple comparison test was used. When two different factors were present in the analysis, differences between groups were evaluated by two-way ANOVA) corrected for multiple comparisons using Sidak's multiple comparison test. Further information about type of test and number of mice used in each experiment, can be found in figure legends. Graphs with multiple time points were analysed with a simple linear regression. A p value <0.05 was considered significant (*/# for $p < 0.05$, **/## for $p < 0.01$ and ***/### for $p < 0.001$).